**– For internal NASA and partners use only –**

# Lunar Impact Ejecta Benchmark and Models

*Anthony M. DeStefano*
NASA, MSFC, EV44

September 29, 2020

## Contents

# List of Figures

# List of Tables

# 1 Executive Summary

# 2 Characteristics of the 17 March 2013 Event

## 2.1 LRO Observations: Robinson et al. 2015

Here we summarize the findings from *Robinson et al.* [2015]. Their assessment used the impact-scaling model of *Holsapple* [1993] to constrain the impact event parameters, with a fixed rim-to-rim crater diameter.

### 2.1.1 Crater Morphology

The March 2013 crater has a rim-to-rim diameter of $D_{rim} = 18.8^{+1.1}_{-1.2}$ m with a depth of approximately 2-3 m. The transient crater diameter was estimated to be $D = 14$ m, see Figure 1 for an illustration.

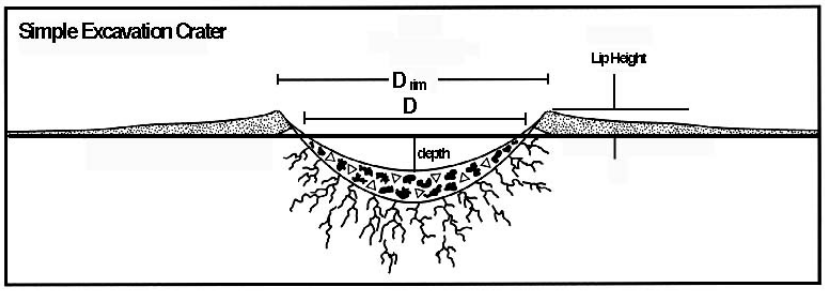


Figure 1: Example of a simple excavation crater, http://keith.aa.washington.edu/craterdata/scaling/index.htm.

### 2.1.2 Impact Event Parameters

Impactor densities were chosen to be either cometary 1 g/cm$^3$, chondritic 3.4 g/cm$^3$, or iron-nickle 6 g/cm$^3$ with plausible impact velocities of 5-60 km/s. The diameter of the impactor was between 0.28 and 1.10 m with a mass between 33 and 702 kg. For this given range of impact velocities and densities, the kinetic energy of the impactor was between $6.4 \times 10^9$ J and $6.0 \times 10^{10}$ J.

## 2.2 MEO Observations: Moser et al. 2014, ACM

Here we summarize the findings from *Moser et al.* [2014]. They used both Gault's crater scaling law [*Gault*, 1974] and Holsapple's online calculator [*Holsapple*, 1993] in their analysis.

#### 2.2.1 Correlation with Meteor Activity

*Moser et al.* [2014] found correlation with the Virginid meteor shower complex (EVI/NVI) with an observed meteor shower on 17 March 2013 and the lunar impact that was seen by NASA MSFC. According to the Meteor Data Center, the eta Virginids, EVI, have a speed of 26.6 km/s to 34.2 km/s and the Northern March Virginids, NVI, have a speed of 23.0 km/s. However, given the cluster of five fireballs that were seen on 17 March 2013, the speed was $v_g = 25.6 \pm 0.8$ km/s and matched closer to the EVI orbital elements. The Tisserand number was $3.1 \pm 0.2$, which is right on the line of being either cometary ($< 3$) or asteroidal ($> 3$). It was found that the lunar impact angle from the horizontal was $\theta_h = 56°$ for a Virginid meteor.

#### 2.2.2 Impact Event Parameters

Assuming a regolith density of $\rho_t = 1500$ kg/m$^3$, a porosity of 40%, and cohesion strength of 0.1 Mpa, the impactor densities ranged from 1000 kg/m$^3$ to 3300 kg/m$^3$, the mass was between 11 kg and 66 kg, and the kinetic energy ranged from $3.6 \times 10^9$ J to $2.2 \times 10^{10}$ J. The duration of the impact was estimated to be 1.03 s with a nominal diameter of $22 \pm 3$ cm, assuming $\rho_p = 3000$ kg/m$^3$.

#### 2.2.3 Luminous Efficiency

From *Moser et al.* [2014], if we assume the impactor was associated with the Virginids, the luminous efficiency $\eta_\lambda$ is in the range $7.5^{+4.5}_{-2.5} \times 10^{-4} < \eta_\lambda < 1.5^{+0.8}_{-0.5} \times 10^{-3}$, depending on the regolith density, $1500$ kg/m$^3 < \rho_t < 2100$ kg/m$^3$, and impactor density, $1000$ kg/m$^3 < \rho_t < 3300$ kg/m$^3$. This range of luminous efficiencies is consistent with *Bouley et al.* [2012] ($\eta_\lambda = 5 \times 10^{-4}$) and *Moser et al.* [2011] ($\eta_\lambda = 1.3 \times 10^{-3}$).

# 3 Lunar Regolith Properties

# 4 Spheral Benchmark of 17 March 2013 Event

## 4.1 Getting Started and Running on Computer Clusters

### 4.1.1 Installing on MEO Cluster

```
References:
If gcc is too old, follow this if you have CentOS:
https://ahelpme.com/linux/centos7/how-to-install-new-gcc-and-
    development-tools-under-centos-7/


To install Spheral and test installation:

cd
mkdir Spheral
```

```
mkdir github-Spheral
cd github-Spheral
git clone https://github.com/jmikeowen/spheral
cd spheral/src/
scl enable devtoolset-7 bash
./boot
mkdir BUILD
cd BUILD
../configure --prefix=/home/adestefa/Spheral --with-opt=3 --
    with-compilers=gnu --with-dbc=none
make -j 20
cd /home/adestefa/github-Spheral/spheral/tests
/home/adestefa/Spheral/bin/ats -n 20 -e /home/adestefa/Spheral
    /bin/python integration.ats



To install VisIt:

cd
mkdir download-visit
cd download-visit/
wget http://portal.nersc.gov/project/visit/releases/2.13.3/
    visit2_13_3.linux-x86_64-rhel7.tar.gz
wget http://portal.nersc.gov/project/visit/releases/2.13.3/
    visit-install2_13_3
chmod 755 visit-install2_13_3
./visit-install2_13_3 2.13.3 linux-x86_64-rhel7 /home/adestefa
    /visit-2.13.3
cd
echo "export PATH=$PATH:/home/adestefa/visit-2.13.3/bin" >> .
    bashrc
```

#### 4.1.2 Running on MEO Cluster

#### 4.1.3 Running on LLNL Cluster

The connection and login details described below is assumed to be on a Windows machine.

1. Connect to VPN using Cisco AnyConnect Secure Mobility Client
   - VPN name: vpn.llnl.gov
   - Group name: llnl.vpnc
2. Login with OUN (destefano2) and CZ PIN + token # (RSA SecurID)
3. SSH into LLNL server head node using Putty

- Host name: rzgw.llnl.gov
- Option: Connection → SSH → X11 → Enable X11 forwarding[1]
- Option: X display location → localhost:0
- Login: LC username (destefan)
- Password: RZ PIN + token # (RZ)

4. SSH into RZ specific server
   - ssh -XY destefan@rztopaz
   - Password: RZ PIN + token # (RZ)
5. Check current jobs for a user
   - squeue -u <username>
   - Add - -start to see begin ETA
6. Load Spheral module
   - ml Spheral/exp
7. Debug Spheral Python script
   - srun -n <# of CPUs, max 36 per node> -p pdebug python -i <python_script.py>
   - Add any variable definitions after the python_script.py, such as - -impactAngle=56, - -rImpactor=25.2, etc. See the halfSphere_amdvX.py file for more variable options.
8. Grab compute nodes for continuous debugging
   - mxterm <# of nodes, max 8> <# of CPUs, =36×# of nodes, max 288> <time, max 60 (minutes)> -q pdebug
   - After nodes have been grabbed, do steps 6 and 7 as before
9. Submit batch script
   - msub <script.msub>
10. Check drive space quota
    - quota -v

[1] Need to download either VcXsrv (works better), or Xming. In VcXsrv, which will be called VLaunch on the desktop, need to deselect **Native opengl** on the last tab.

### 4.2 Porosity $\phi_0$ Study

### 4.3 Max Strength $Y_m$ Study

## 5 Spheral Based Lunar Ejecta Modeling

## 6 MEM3 Based Lunar Ejecta Modeling

The Meteoroid Engineering Model (MEM) describes the sporadic meteoroid complex, or the background meteoroid environment, and does not include meteor showers. The impactor masses range from $1$ $\mu$g to $10$ g. Larger impactor masses must be dealt with differently [e.g., see *Neukum et al.*, 2001; *Brown et al.*, 2002], *which we omit here for now*[2]. We use output from MEM in order to estimate the number of particles per area per year greater than a certain mass (or the particle flux mass spectrum) due to secondary ejecta from meteoroid impacts on the Moon. The risk due to impacts on the Moon is driven by secondary ejecta and not the primary meteoroid flux.

We begin by first describing the algorithm at which we plan to use to compute the particle flux mass spectrum at a given point on the Moon. In essence, the algorithm is based on the reverse Monte-Carlo idea. We then go into detail about how to compute each step of the algorithm, either borrowing from the literature or making our own derivations.

### 6.1 Algorithm

1. For a given location on the Moon, compute the particle flux mass spectrum
2. For each source location
   - Defines the distance $D$ from the source required to compute the ejecta velocity $v = v(D, \gamma)$.
3. For each ejecta angle $\gamma$
   - Completely defines the ejecta velocity $v = v(D, \gamma)$
4. For each meteoroid impact angle $\alpha$ (from MEM output)
   - At the moment, we will sum over the azimuthal angle and assume isotropic azimuthal seconday ejecta (this is not the case for impact angles less than $30^\circ$ from the horizon).
5. For each meteoroid impact speed $U$
6. For each impactor density $\delta$
   - We only need to compute this once for each target material, and can factor out as a constant. The density is given as an output in MEM.

[2] At some point we will need to account for impactor masses larger than 10 g in order to understand the tail of the distribution in terms of the risk analysis.

7. For each impactor mass $m_p$
   - We can integrate this out. At first glance, we will get a list of hypergeometric functions, but we only need to evaluate these once and factor out as a constant. The mass distribution is given in MEM Eq. (2.1).
8. For each ejecta particle size $m_e$
   - We can integrate the particle size distribution, but we will need to keep track of each mass size $m_e$.

## 6.2 Regolith Size Distribution

For relatively small impact sizes (craters $< 30 - 50$ m), we can generally assume the secondary ejecta follows that of the original regolith. The cumulative distribution function (CDF) of the particle sizes can be fit to many observations, as shown in Figure 2.

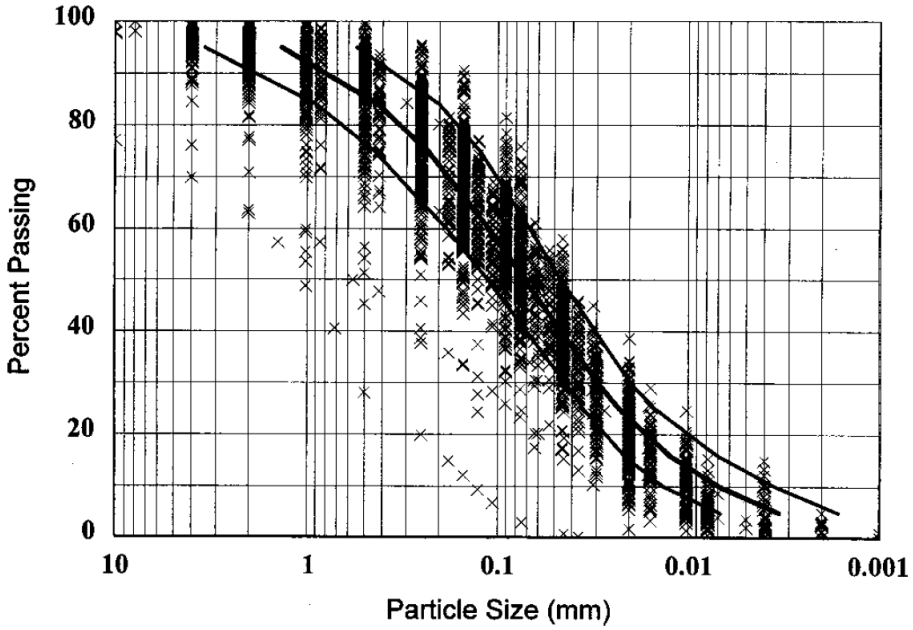


Figure 2: Geotechnical particle size distribution: middle curve showing the average distribution; left-hand and right-hand curves showing $\pm 1$ standard deviation [*Carrier III*, 2003]. Note, that the percent passing is normalized by mass and not particle number [see *Carrier*, 1973].

The digitized data from Figure 2 is shown in Table 1.

Table 1: Digitized data points from Figure 2, see *Carrier III* [2003].

| Particle Diameter (mm) | Cumulative Percent by Mass |
|---|---|
| 0.003380248352585 | 5.17682028091534 |
| 0.003794441295246 | 6.09401642297017 |
| 0.00451292465605 | 7.2776812909626 |
| 0.0053674729594 | 8.4354410787182 |
| 0.006383732464611 | 9.71063723021409 |
| 0.007592176031253 | 11.2086170717467 |
| 0.009029116435596 | 12.9190185712213 |
| 0.010737989052827 | 14.65100763756 |
| 0.012769865152208 | 16.6247774527757 |
| 0.015185144104918 | 19.116648872728 |
| 0.018057261192048 | 21.6025237463292 |
| 0.02136872870221 | 24.2948870610798 |
| 0.025044648784976 | 27.0334149904509 |
| 0.029494364580794 | 29.8741284657866 |
| 0.033098954040892 | 32.8807708128992 |
| 0.037145453042138 | 35.6150479687852 |
| 0.042499223173782 | 38.2089250804786 |
| 0.048155933590968 | 41.1181012805662 |
| 0.054042887826956 | 43.8970091889745 |
| 0.060942690951498 | 46.6685810695819 |
| 0.068720899309714 | 49.7075873197331 |
| 0.077869796000019 | 52.4248808897808 |
| 0.087812953450079 | 55.0874612212659 |
| 0.098550426314892 | 57.6779504306929 |
| 0.112206724061769 | 60.6265864834011 |
| 0.127759476997186 | 63.3415731364729 |
| 0.145465039759366 | 66.2037864789212 |
| 0.168035843630453 | 69.131911259623 |
| 0.19411176280305 | 71.9484525505802 |
| 0.222083419318477 | 74.7285290349147 |
| 0.259044020108005 | 77.2129935126797 |
| 0.30803890584547 | 79.7150699642405 |
| 0.366294873918129 | 82.3305792671413 |
| 0.435590409221425 | 84.5720349114709 |
| 0.518029785192508 | 86.3256115446736 |
| 0.616085725364177 | 87.9108051563369 |
| 0.732705596850257 | 89.4631856663669 |
| 0.871382022892136 | 91.1718601604924 |
| 1.03629488039837 | 92.9535006306183 |
| 1.23245384670266 | 94.5235829454768 |

In order to parameterize the CDF from Figure 2, we make a fit to the model equation

$$C_{\text{Moon}} = 1 - \exp\left(\frac{-1}{ax^b + cx^d}\right), \tag{6.1}$$

which is an exponential distribution with two scales defined by $a$ and $c$, with $x$ in units of mm. In SciDAVis, we make the fit with the x-axis on a logarithmic scale to give equal weight to both small and large scaled particles. The results for the curve fit are shown in Figure 3. We found that a simple exponential distribution with a single scale was insufficient, hence the reason we opted for a two-scaled exponential distribution.

```
[12/30/2019 5:40:09 PM          Plot: "Graph2"]
Non-linear fit of dataset: Table2_2, using function: 100*(1-exp(-1/(a*(10^x)^b+c*(10^x)^d)))
Y standard errors: Unknown
Nelder-Mead Simplex algorithm with tolerance = 0.0001
From x = -2.482108151 to x = 0.134259956
a  = 0.0548044684398436 +/- 0.00569348851446585
b  = -1.01472478485333 +/- 0.0196858460040614
c  = 0.337499285612252 +/- 0.0049924392579481
d  = -0.251808155531636 +/- 0.0188844274561765
--------------------------------------------------------------------------------
Chi^2 = 8.25978651917647
R^2 = 0.999849854428033
--------------------------------------------------------------------------------
Iterations = 89
Status = success
--------------------------------------------------------------------------------
```

Figure 3: Non-linear fit of Figure 2 (the average distribution) with Eq. 6.1 in SciDAVis, giving the constants for $a$, $b$, $c$, and $d$.

To compute the probability distribution function (PDF), we can simply take the derivative of the CDF with respect to $x$, which results in the following equation:

$$P_{\text{Moon}} = -A\frac{abx^{b-1} + cdx^{d-1}}{(ax^b + cx^d)^2} \exp\left(\frac{-1}{ax^b + cx^d}\right), \tag{6.2}$$

where $A$ is the normalization constant. In theory, this should be equal to 1, but since we are not taking our particle size from 0 to infinity, we need to compute the value of $A$. If we assume the particle size can range from $0.001$ mm to $10$ mm, then $A = 1.02218$.

In order to compare with NASA SP-8013 [*Cour-Palais*, 1969], we first must convert the distribution function normalized by number and not mass. We can then write

$$N_{ej}(x) \sim \int_x^\infty \frac{dx}{m(x)} \frac{d(C_{\text{Moon}}(x))}{dx}, \tag{6.3}$$

where $x$ is the particle diameter, and

$$m(x) = \frac{\pi}{6}\rho x^3. \tag{6.4}$$

Instead of fitting $C_{\text{Moon}}$ to Figure 2 directly, we will approximate using a power-law interpolation technique such that

$$C_{\text{Moon}}(x) = y_i \left( \frac{x}{x_i} \right)^{b_i}, \tag{6.5}$$

where

$$b_i = \frac{\log(y_{i+1}/y_i)}{\log(x_{i+1}/x_i)}, \tag{6.6}$$

and where $x_i \leq x \leq x_{i+1}$, for data $x_i$ from Figure 2 (also shown in Table 1). Therefore, we can write Equation (6.3) as

$$N_{ej}(x) \sim \frac{6}{\pi\rho} \frac{b_i}{3 - b_i} \frac{y_i}{x_i^{b_i}} x^{b_i - 3}. \tag{6.7}$$

If we want to normalize Equation (6.7) to unity for a certain size $x_{\text{norm}}$, we then have

$$N_{ej}(x) = \frac{b_i(3 - b_n)}{b_n(3 - b_i)} \frac{x_n^{b_n}}{x_i^{b_i}} \frac{y_i}{y_n} \frac{x^{b_i - 3}}{x_{\text{norm}}^{b_n - 3}}, \tag{6.8}$$

where $x_n \leq x_{\text{norm}} \leq x_{n+1}$.

If we apply the method of Equation (6.8) to the Carrier 2003 data shown in Table 1 and make a fit using a double power-law expression given by

$$N_{ej}(x) = \frac{A}{\left(\frac{x}{a}\right)^b + x^d}, \tag{6.9}$$

then the fit parameters can be computed as shown in Figure 4.

```
[9/23/2020 4:38 PM          Plot: "Graph2"]
Non-linear fit of dataset: Table2_2, using function: log10( A/( (10^x/a)^b + (10^x)^d) )
Y standard errors: Unknown
Scaled Levenberg-Marquardt algorithm with tolerance = 0.0001
From x = -2.47105139019728 to x = 0.090770664665162
A  = 0.00921624902003821 +/- 0.0046037913480369
a  = 0.346681782684812 +/- 0.0532546027488427
b  = 3.60486296421154 +/- 0.0789704288933391
d  = 2.32993070045899 +/- 0.096749147779981
------------------------------------------------------------------------------
Chi^2 = 0.172121195592017
R^2 = 0.999116143889293
------------------------------------------------------------------------------
Iterations = 0
Status = success
------------------------------------------------------------------------------
```

Figure 4: Non-linear fit of Table 1 with Eq. 6.9 in SciDAVis, giving the constants for $A$, $a$, $b$, and $d$.

## 6.3 Ejected Mass from an Impactor

From *Housen and Holsapple* [2011], we can compute the mass ejected faster than $v$ in terms of impactor properties, given by

$$M(v;\rho;m,\delta,U,\alpha) = M(>v) = C_4 m \left[\frac{v}{U\Theta(\alpha)}\left(\frac{\rho}{\delta}\right)^{\frac{3\nu-1}{3\mu}}\right]^{-3\mu}, \tag{6.10}$$

where

- $v$: secondary ejecta speed,
- $\rho$: target density,
- $m$: projectile mass,
- $\delta$: projectile density,
- $U$: projectile speed,
- $\alpha$: projectile impact angle (from horizon),

and

$$C_4 = \frac{3k}{4\pi}C_1^{3\mu}, \tag{6.11}$$

where the constants $k$, $C_1$, $\nu$, and $\mu$ depend on the specific material properties, see Table 3 of *Housen and Holsapple* [2011]. The impact angle modification equation $\Theta(\alpha)$ can be chosen to be

$$\Theta(\alpha) = \begin{cases} 1 \\ \sin\alpha \\ \sin(\sqrt{\alpha_0^2+\alpha^2}),\ \alpha_0 \sim 5^\circ - 15^\circ. \end{cases} \tag{6.12}$$

For the ejected mass that is in a given velocity range, we can define $\Delta M(v_2, v_1)$ as

$$\Delta M(v_2, v_1) = M(>v_2) - M(>v_1). \tag{6.13}$$

## 6.4 Ejecta Mass Distribution Function

The mass ejected from the crater, $M(>v)$, from Eq. (6.10), is the total mass ejected from an impact at velocities greater than $v$. However, we would like to know how this ejecta is distributed in speed and solid angle so we can map the ejecta to a particular surface location on the Moon. We can then set Eq. (6.10) in terms of the integral over the distribution functions of speed and solid angle as

$$M(>v) = \int_v^\infty \int_0^{2\pi} \int_0^{\pi/2} \sin\alpha d\alpha d\beta dv' F(\alpha)G(\beta)H(v'), \tag{6.14}$$

where $\alpha$ is the zenith angle, $\beta$ is the azimuth angle, and $v$ is the ejecta speed. Just to note, at the secondary impact location, the zenith angle will be the same as the ejected zenith angle. However, the azimuth angle (or bearing) will be modified due to travel across the spherical surface, see Section 6.10.

### 6.4.1 Zenith Distribution Function

For the angular dependent terms $F(\alpha)$ and $G(\beta)$, they technically should depend on speed as well as particle size [e.g., *Rival and Mandeville*, 1999]. For simplicity, we will assume the angular distribution is independent of speed and particle size but will be dependent on impact zenith and azimuth angle with respect to the bearing.

Adopting the zenith and azimuth distributions from *Rival and Mandeville* [1999], we have the following equations: The zenith distribution is given by

$$F(\alpha) = \frac{1}{\sigma\sqrt{2\pi}} \exp\left[-\frac{(\alpha - \alpha_{max})^2}{2\sigma^2}\right], \tag{6.15}$$

where $\alpha_{max}$ is defined as

$$\alpha_{max} = \begin{cases} \frac{\alpha_{max60} - \alpha_{max0}}{\pi/3}\alpha_i + \alpha_{max0} \text{ for } \alpha_i \leq \pi/3 = 60^\circ \\ \alpha_{max60} \text{ for } \alpha_i > \pi/3 = 60^\circ \end{cases}, \tag{6.16}$$

for $\alpha_i$ the impact zenith angle, and [see *Miller*, 2017]

$$\alpha_{max0} = \frac{\pi}{6} = 30^\circ, \tag{6.17}$$

$$\alpha_{max60} = \frac{4\pi}{9} = 80^\circ, \tag{6.18}$$

$$\sigma = \frac{\pi}{60} = 3^\circ, \tag{6.19}$$

where the peak ejecta angle is shifted from $30^\circ$ of zenith for a normal impact to $80^\circ$ of zenith for oblique impacts ($> 60^\circ$).

**Alternative Zenith Distribution:** To complete the integral over the zenith distribution, namely

$$\int_{\alpha_0(v)}^{\alpha_1(v)} d\alpha \sin\alpha F(\alpha), \tag{6.20}$$

we need to choose a distribution function for $F(\alpha)$ to allow for analytic solutions. We will therefore look for an alternate distribution from Eq. (6.15), given by the form

$$F(\alpha) = (1 - \cos\alpha)^{1/a} \cos^a \alpha, \tag{6.21}$$

where the exponent $a$ can be defined in terms of the peak angle $\alpha_{max}$ as

$$a^2 = \frac{\cos\alpha_{max}}{1 - \cos\alpha_{max}} = \frac{\cos\alpha_{max}}{2\sin^2(\alpha_{max}/2)}, \tag{6.22}$$

such that $F'(\alpha_{max}) = 0$ and $F''(\alpha_{max}) < 0$.

In order to compare with experiments for the peak angle $\alpha_{max}$, we can use Figure 18 of *Gault and Wedekind* [1978] as a proxy to our model of $\alpha_{max}$, as a function

of the azimuth angle. Using a third order polynomial for both fits to the downstream and upstream angles given in Table 2, we arrive at

$$\alpha_{max}(\beta - \beta_i = \pi) = 0.0003\alpha_i^3 - 0.036\alpha_i^2 + 1.5206\alpha_i + 20, \text{ downstream} \quad (6.23)$$

$$\alpha_{max}(\beta - \beta_i = 0) = -0.00042\alpha_i^3 + 0.0236\alpha_i^2 + 0.129\alpha_i + 20, \text{ upstream} \quad (6.24)$$

in units of degrees, where $\beta_i$ is the impact azimuth angle, $\beta$ is the ejecta azimuth angle, and $\alpha_i$ is the impact zenith angle. For other values of $\beta - \beta_i$, we can write a complete function as

$$\alpha_{max}(\beta) = \alpha_{max}(\beta - \beta_i = \pi) \cdot \sin^2\left(\frac{\beta - \beta_i}{2}\right) + \alpha_{max}(\beta - \beta_i = 0) \cdot \cos^2\left(\frac{\beta - \beta_i}{2}\right), \quad (6.25)$$

or rewriting we have

$$\alpha_{max}(\beta) = \frac{\alpha_{max,0} + \alpha_{max,\pi}}{2} - \frac{\alpha_{max,\pi} - \alpha_{max,0}}{2}\cos(\beta - \beta_i), \quad (6.26)$$

and solving for $\beta - \beta_i$, after setting $\alpha_{max}(\beta)$ to zero,

$$\arccos\left(\frac{\alpha_{max,0} + \alpha_{max,\pi}}{\alpha_{max,\pi} - \alpha_{max,0}}\right) = \beta - \beta_i. \quad (6.27)$$

As a simplification, we can approximate the $\cos(\beta - \beta_i)$ term as (note, this is not a Taylor series)

$$\cos(\beta - \beta_i) \sim 1 - \left|\frac{\beta - \beta_i}{\pi/2}\right|, \quad (6.28)$$

for $-\pi \leq \beta - \beta_i \leq \pi$ such that $\cos\alpha_{max}$ becomes

$$\cos\alpha_{max} \sim \cos\left[\alpha_{max,0} + \frac{\alpha_{max,\pi} - \alpha_{max,0}}{\pi}|\beta - \beta_i|\right] \quad (6.29)$$

Table 2: Cone angles of upstream and downstream of impact derived from Figure 18 of *Gault and Wedekind* [1978].

| Impact Zenith Angle | Upstream Zenith Angle | Downstream Zenith Angle |
|---|---|---|
| 0 | 20 | 20 |
| 15 | 24 | 35 |
| 30 | 35 | 45 |
| 45 | 28 | 40 |
| 60 | 13 | 54 |
| 75 | -35 | 66 |

Using Table 2 as a fit for the peak angle $\alpha_{max}$ is an approximation since the tabular data is only for a specific snapshot of the ejecta at a side view, $90^\circ$ from the impact direction. The zenith distribution should also be a function of the ejecta speed, but we

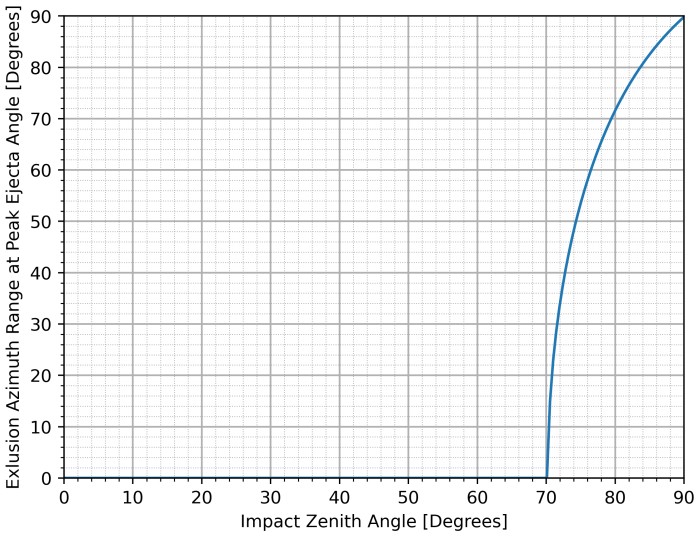


Figure 5: For larger impact angles that are more grazing to the surface, the zenith and azimuth ejecta distributions become asymmetric. Starting at $70^\circ$, the peak ejecta angle $\alpha_{max}$ becomes negative in an exclusion range, as shown in the figure. This means that the $-\alpha_{max} \rightarrow \alpha_{max}$ and $\beta - \beta_i \rightarrow \beta - \beta_i + \pi$. In this model, for impact angles near $90^\circ$, most of the ejecta is concentrated in the downstream direction.

do not make this assumption for the sake of simplicity. According to this model, starting around $60^\circ - 70^\circ$, there is a region of exclusion for a part of the zenith distribution upstream of the impact, see Figure 5.

Next, we can do a variable substitution (chosen so the domain of the zenith angle to the new variable goes from $\alpha \in [0, \pi/2]$ to $x \in [0, 1]$)

$$1 - x = \cos\alpha, \tag{6.30}$$

$$dx = \sin\alpha d\alpha, \tag{6.31}$$

so that Eq. (6.20) becomes

$$\int_{x_0(v)}^{x_1(v)} dx x^{1/a}(1-x)^a, \tag{6.32}$$

where the equations $x_0(v)$ and $x_1(v)$ are a linear function of $v$ and an implicit function of the distances $D_0$ and $D_1$, respectively. The integral in Eq. (6.32) is the incomplete beta function

$$\int_{x_0(v)}^{x_1(v)} dx x^{1/a}(1-x)^a = \beta(x_1(v); 1/a+1, a+1) - \beta(x_0(v); 1/a+1, a+1). \tag{6.33}$$

Note that the normalization term for $\alpha \in [0, \pi/2]$ is given by

$$\int_0^{\pi/2} d\alpha \sin\alpha F(\alpha) = \beta(1/a+1, a+1) = \frac{\Gamma(1/a+1)\Gamma(a+1)}{\Gamma(a+1/a+2)}, \tag{6.34}$$

which includes ejecta at speeds greater than the escape speed.

For small differences in $D_0$ and $D_1$, we can roughly assume small differences[3] in $x_0(v)$ and $x_1(v)$ so that we can write Eq. (6.33) in terms of a derivative, where we evaluate the derivative at the midpoint

$$\begin{aligned}
&\beta(x_1(v); 1/a+1, a+1) - \beta(x_0(v); 1/a+1, a+1) \\
=&\frac{\beta(x_0(v)+\Delta x; 1/a+1, a+1) - \beta(x_0(v); 1/a+1, a+1)}{\Delta x}\Delta x \\
\approx&\Delta x \frac{d}{d(x_0(v))}\beta(x_0(v); 1/a+1, a+1)\Big|_{x_0(v)\to x_0(v)+\Delta x/2} \\
=&\Delta x \left[1-x_0(v)\right]^a x_0^{1/a}(v)\Big|_{x_0(v)\to x_0(v)+\Delta x/2} \\
=&\Delta x(v)\left[1-\frac{x_0(v)+x_1(v)}{2}\right]^a\left[\frac{x_0(v)+x_1(v)}{2}\right]^{1/a},
\end{aligned} \tag{6.35}$$

where $\Delta x(v) = x_1(v) - x_0(v)$, and (note, the $v$'s are normalized by $v_{esc}$, emitted for clarity)

$$x_0(v) = m_0 v + b_0, \tag{6.36}$$
$$x_1(v) = m_1 v + b_1, \tag{6.37}$$
$$\Delta x(v) = (m_1 - m_0)v + b_1 - b_0. \tag{6.38}$$

The coefficients $m_0, m_1$ and $b_0, b_1$ are implicit functions of the distances $D_0, D_1$. For the $j-$th distance $D_j$ and the $i-$th speed $v_i$, the $m$ and $b$ coefficients can be written as

$$m^{\pm}_{j,i} = \frac{v_{i+1} - v_i}{x^{\pm}_{j,i+1} - x^{\pm}_{j,i}}, \tag{6.39}$$
$$b^{\pm}_{j,i} = v_i - m^{\pm}_{j,i} \cdot x^{\pm}_{j,i}, \tag{6.40}$$

where

$$x^{\pm}_{j,i} = 1 - \cos\alpha^{\pm}_{j,i}, \tag{6.41}$$

for

$$\cos^2\alpha^{\pm}_{j,i} = \frac{v_i^2 + \tan^2\left(\frac{D_j}{2r_m}\right)(2v_i^2-1) \pm \sqrt{v_i^4 + \tan^2\left(\frac{D_j}{2r_m}\right)(2v_i^2-1)}}{2v_i^2\left(1+\tan^2\left(\frac{D_j}{2r_m}\right)\right)}, \tag{6.42}$$

[3] If $\Delta x$ is not small, then we can partition the $x$ range into smaller pieces so that $\Delta x$ is small, which will be the case in almost all circumstances.

taking the positive root, $\cos\alpha_{j,i}^{\pm} = +\sqrt{\cos^2\alpha_{j,i}^{\pm}}$, since $\alpha \in [0, \pi/2]$. Other useful transformed equations are

$$\tan\left(\frac{D_j}{2r_m}\right) = \frac{2v_i^2(1-x_{j,i}^{\pm})\sqrt{x_{j,i}^{\pm}(2-x_{j,i}^{\pm})}}{1-2v_i^2x_{j,i}^{\pm}(2-x_{j,i}^{\pm})}, \tag{6.43}$$

from Eq. (6.94), and

$$v_i = \frac{1}{\sqrt{2(1-x_{j,i}^{\pm})\sqrt{x_{j,i}^{\pm}(2-x_{j,i}^{\pm})}\cot\left(\frac{D_j}{2r_m}\right) + 2x_{j,i}^{\pm}(2-x_{j,i}^{\pm})}}, \tag{6.44}$$

from Eq. (6.97). Solving for $x_{j,i}^{\pm}$ in either equation, we can now write $x$ explicitly in terms of the distance $D$ and ejecta speed $v$ as

$$x_{j,i}^{\pm} = 1 - \sqrt{\frac{v_i^2 + \tan^2\left(\frac{D_j}{2r_m}\right)(2v_i^2-1) \pm \sqrt{v_i^4 + \tan^2\left(\frac{D_j}{2r_m}\right)(2v_i^2-1)}}{2v_i^2\left[1+\tan^2\left(\frac{D_j}{2r_m}\right)\right]}}. \tag{6.45}$$

For a given distance, the domain of $x$ is given by (for $v$ up to 1)

$$x_{j,i}^{\pm} \in \left(1-\cos\left(\frac{D_j}{4r_m}\right), 1\right), \tag{6.46}$$

and the domain of $v$ is given by

$$v_i \in \begin{cases} \left(\left[1+\left|\cos\left(\frac{D_j}{2r_m}\right)\right|\cot\left(\frac{D_j}{2r_m}\right)+\sin\left(\frac{D_j}{2r_m}\right)\right]^{-1/2}, 1\right) & \text{for } D_j < \pi r_m \\ \left(\frac{\sqrt{2}}{2}, 1\right) & \text{for } D_j \geq \pi r_m \end{cases} \tag{6.47}$$

where the value of $x_{j,i}^{\pm}$ at the minimum of $v_i$ is

$$x_{j,i}^{\pm} = 1 - \sqrt{\frac{1-\sin\left(\frac{D_j}{2r_m}\right)}{2}} \tag{6.48}$$

The two domains in Eqs. (6.46) and (6.47) define the region of interest, and allow for the integration to begin at the correct outermost boundary lines.

There are three regions of the zenith angle-space, and hence the $x$-space, where we have:

Region I: For all valid distances $D_j$ and $D_{j+1}$, use $m_{j,i}^{+}$, $b_{j,i}^{+}$, $m_{j+1,i}^{+}$ and $b_{j+1,i}^{+}$

Region II: For $D_j < \pi r_m$ and all $D_{j+1}$, use $m_{j,i}^{-}$, $b_{j,i}^{-}$, $m_{j+1,i}^{+}$ and $b_{j+1,i}^{+}$

Region III: For $D_j < \pi r_m$ and $D_{j+1} < \pi r_m$, use $m_{j,i}^{-}$, $b_{j,i}^{-}$, $m_{j+1,i}^{-}$ and $b_{j+1,i}^{-}$

### 6.4.2 Azimuth Distribution Function

The azimuth distribution shown below is given by [*Rival and Mandeville*, 1999]

$$G(\beta) = \begin{cases} \frac{1}{2\pi}\left[\frac{3\alpha_i}{2\pi-3\alpha_i}\cos(\beta-\beta_i)+1\right] & \text{for } \alpha_i \leq \pi/3 = 60^\circ \\ \frac{1}{\sigma'\sqrt{2\pi}}\exp\left[-\frac{(\beta-\beta_i)^2}{2\sigma'^2}\right] & \text{for } \alpha_i > \pi/3 = 60^\circ \end{cases}, \tag{6.49}$$

where

$$\sigma' = \frac{\pi}{36} = 5^\circ, \tag{6.50}$$

for $\beta_i$ the impact azimuth angle + $\pi$.

**Alternative Azimuth Distribution:** The piece-wise function defined in Equation (6.49) for the azimuth distribution is correctly normalized for impact zenith angles $\alpha_i \leq 60^\circ$, however for angles greater than $60^\circ$, the function is not continuous across the boundary $\beta = 2\pi \rightarrow 0$. We would also like a continuous function across the piece-wise boundary as well.

Our proposed azimuth distribution is as follow. We will use the $\alpha_i \leq 60^\circ$ functional form in Equation (6.49), but we will have a different large-angle expression. The new azimuth distribution is defined as

$$G(\beta) = \begin{cases} \frac{1}{2\pi}\left[\frac{3\alpha_i}{2\pi-3\alpha_i}\cos(\beta-\beta_i)+1\right] & \text{for } \alpha_i \leq \pi/3 = 60^\circ \\ \frac{1}{A}\left[\exp\left[-\frac{(\beta-\beta_i-2(\alpha_i-\alpha_{i,0}))}{\pi b}\right]+\exp\left[-\frac{(\beta-\beta_i+2(\alpha_i-\alpha_{i,0}))}{\pi b}\right]\right] & \text{for } \alpha_i > \pi/3 \end{cases}, \tag{6.51}$$

where

$$b = \frac{0.05-1}{\pi/2-\pi/3}(\alpha_i-\alpha_{i,0})+1 = \frac{3}{10\pi}(\alpha_i-\alpha_{i,0})+1, \tag{6.52}$$

and

$$\alpha_{i,0} = \pi/3. \tag{6.53}$$

For the second case, we empirically include information about the *butterfly pattern* that is seen for highly oblique impact angles [e.g., *Shuvalov*, 2011]. The size of the impactor will affect the spread of the butterfly pattern, but we assume a certain spread profile for all impactor sizes.

The normalization[4] constant for the $\alpha_i > \pi/3$ case is

$$A = \sqrt{b}\pi\left[\text{erf}\left(\frac{\pi+2(\alpha_i-\alpha_{i,0})}{\sqrt{\pi b}}\right)+\text{erf}\left(\frac{\pi-2(\alpha_i-\alpha_{i,0})}{\sqrt{\pi b}}\right)\right], \tag{6.54}$$

when integrating $\beta-\beta_i$ from $-\pi$ to $\pi$. However, when integrating the outgoing secondary azimuth angle $\beta$ with respect to the impact azimuth angle $\beta_i$ when there is an

[4]Please note that this is not the exact normalization. This is assuming that the altitude distribution does not depend on the azimuth, which is not the case. We only include this here to *help* the overall normalization once we calculate it, which will have to be done by a numerical integral.

exclusion zone defined by $\pm\Delta\beta_{ez}$, the normalization constant is

$$A = \sqrt{b}\pi \left[ \text{erf}\left( \frac{\pi - \Delta\beta_{ez} + 2(\alpha_i - \alpha_{i,0})}{\sqrt{\pi b}} \right) + \text{erf}\left( \frac{\pi - \Delta\beta_{ez} - 2(\alpha_i - \alpha_{i,0})}{\sqrt{\pi b}} \right) \right], \quad (6.55)$$

which is appropriate for any $\alpha_i > \pi/3$ for an exclusion zone $\Delta\beta_{ez}$ given by (using Eq. (6.29) = $\pi/2$)

$$\Delta\beta_{ez} = \begin{cases} \pi \frac{-\alpha_{max,\pi}}{\alpha_{max,0} - \alpha_{max,\pi}}, \text{ for } \alpha_{max,\pi} < 0 \\ 0, \text{ otherwise} \end{cases} \quad (6.56)$$

For $\alpha_i > \pi/3 = 60°$, in order to integrate over a small azimuth range $\beta \in (\beta_0, \beta_1)$
For $\alpha_i \leq \pi/3 = 60°$, integrating over a small range $\Delta\beta = \beta_1 - \beta_0$, the integral is given by

$$\begin{aligned} &\frac{1}{2\pi} \int_{\beta_0}^{\beta_1} d\beta \left[ \frac{3\alpha_i}{2\pi - 3\alpha_i} \cos(\beta - \beta_i) + 1 \right] \\ =&\frac{1}{2\pi} \left[ \Delta\beta + \frac{3\alpha_i}{2\pi - 3\alpha_i} \left[ \sin(\beta_1 - \beta_i) - \sin(\beta_0 - \beta_i) \right] \right]. \end{aligned} \quad (6.57)$$

### 6.4.3 Speed Distribution Function

The speed distribution $H(v')$ is defined by

$$\int_v^\infty dv' H(v') = v^{-3\mu}, \quad (6.58)$$

which is the speed dependent term of Eq. (6.10). We can then solve the speed distribution explicitly as

$$H(v) = 3\mu v^{-(3\mu+1)}. \quad (6.59)$$

To integrate over the velocity distribution, we must take the results from Section 6.4.1 on the zenith distribution function and combine them with the above integral, giving

$$3\mu \int_{v_0}^{v_1} dv v^{-(3\mu+1)} \Delta x(v) \left[ 1 - \frac{x_0(v) + x_1(v)}{2} \right]^a \left[ \frac{x_0(v) + x_1(v)}{2} \right]^{1/a} \quad (6.60)$$

$$=3\mu \int_{v_0}^{v_1} dv v^{-(3\mu+1)} (\Delta m v + \Delta b)(1 - m_{avg} v - b_{avg})^a (m_{avg} v + b_{avg})^{1/a} \quad (6.61)$$

$$= \int_{v_0}^{v_1} dv H_2(v), \quad (6.62)$$

where

$$\Delta m = m_1 - m_0, \tag{6.63}$$
$$\Delta b = b_1 - b_0, \tag{6.64}$$
$$m_{avg} = \frac{m_0 + m_1}{2}, \tag{6.65}$$
$$b_{avg} = \frac{b_0 + b_1}{2}. \tag{6.66}$$

This integral is related to the Appell F1 multivariate hypergeometric function and cannot be simplified to a finite number of single variable hypergeometric functions for generalized values of the exponent $a$. At this time, we will defer to integrate this equation numerically, preferably using the Romberg integration method.

Alternatively, we can attempt to generate an approximation similar to what we did in Sections 6.4.1 and 6.4.2. Taking the Taylor expansion of Equation (6.62) about $v_{avg}$ out to the first term, we have (note, the first term drops out of the integral during integration, so the error is of order $\Delta v^3$)

$$\int_{v_0}^{v_1} dv H_2(v) \sim \int_{v_0}^{v_1} dv[H_2(v_{avg}) + H_2'(v_{avg})(v - v_{avg}) + \dots], \tag{6.67}$$
$$= \Delta v H_2(v_{avg}),$$

$$= 3\mu \Delta v v_{avg}^{-(3\mu+1)}(\Delta m v_{avg} + \Delta b)(1 - m_{avg}v_{avg} - b_{avg})^a (m_{avg}v_{avg} + b_{avg})^{1/a}, \tag{6.68}$$

where

$$\Delta v = v_1 - v_0, \tag{6.69}$$
$$v_{avg} = \frac{v_0 + v_1}{2}. \tag{6.70}$$

### 6.4.4 Normalization Term

In order to relate to the secondary mass ejected faster than $v$, we need the normalization term $\mathcal{M}$ such that

$$M(>v) = \mathcal{M}(\alpha_i, U_i) \int_v^\infty \int_0^{2\pi} \int_0^{\pi/2} \sin\alpha d\alpha d\beta dv' F(\alpha) G(\beta) H(v'). \tag{6.71}$$

Solving for $\mathcal{M}$ and performing the integral over speed $v'$, we have

$$\mathcal{M}(\alpha_i, U_i) = \frac{C_4 m [U_i \Theta(\alpha_i)]^{3\mu} \left(\frac{\delta}{\rho}\right)^{3\nu-1}}{\mathcal{G}(\alpha_i)}, \tag{6.72}$$

where $\mathcal{G}$ is given by ($x = \beta - \beta_i$)

$$\mathcal{G}(\alpha_i) = \int_{-(\pi-\Delta\beta_{ez})}^{\pi-\Delta\beta_{ez}} dx G(x + \beta_i) \frac{\Gamma(1/a+1)\Gamma(a+1)}{\Gamma(a+1/a+2)}, \tag{6.73}$$
$$= 2\int_0^{\pi-\Delta\beta_{ez}} dx G(x + \beta_i) \frac{\Gamma(1/a+1)\Gamma(a+1)}{\Gamma(a+1/a+2)}, \tag{6.74}$$

where $\Delta\beta_{ez}$ and $a$ are given in Eq. (6.56) and Eq. (6.22), respectively. Recall, that $a$ is given by

$$a = \frac{\cos\alpha_{max}}{1-\cos\alpha_{max}} = \frac{\cos\alpha_{max}}{2\sin^2(\alpha_{max}/2)}, \tag{6.75}$$

and where $\alpha_{max}$ is given by

$$\alpha_{max} = \alpha_{max,0} + \frac{\alpha_{max,\pi} - \alpha_{max,0}}{\pi}|x|. \tag{6.76}$$

The $\mathcal{G}$ pre-normalization term can be computed using your favorite numerical integration method, such as Romberg integration.

## 6.5 Algorithm to Integrate Speed-Zenith Space

For the three different possible regions as defined in Section 6.4.1, shown here again for convenience

Region I: For all valid distances $D_j$ and $D_{j+1}$, use $m^+_{j,i}$, $b^+_{j,i}$, $m^+_{j+1,i}$ and $b^+_{j+1,i}$

Region II: For $D_j < \pi r_m$ and all $D_{j+1}$, use $m^-_{j,i}$, $b^-_{j,i}$, $m^+_{j+1,i}$ and $b^+_{j+1,i}$

Region III: For $D_j < \pi r_m$ and $D_{j+1} < \pi r_m$, use $m^-_{j,i}$, $b^-_{j,i}$, $m^-_{j+1,i}$ and $b^-_{j+1,i}$,

there will be a fixed combination of ways the speed-zenith curves will intersect a given speed-zenith bin. For each region, we can assume the following about the slopes of the curves (and hence, the sign of their derivatives):

Region I: Negative,

Region II: Zero,

Region III: Positive.

Our analysis of Region I will be a mirror image of Region III. Region II is trivial in that there is only one case. We will outline the all the cases below for each region.

### 6.5.1 Region I

## 6.6 Meteoroid Projectile Mass Distribution

From the MEM3 User Guide , we get the $g(m)$ flux of meteoroids larger than a limiting mass $m$, originally from *Grün et al.* [1985]. The Grün interplanetary flux equation is given by

$$g(m) = (c_4 m^{\gamma_4} + c_5)^{\gamma_5} + c_6(m + c_7 m^{\gamma_6} + c_8 m^{\gamma_7})^{\gamma_8} + c_9(m + c_{10} m^{\gamma_9})^{\gamma_{10}}, \tag{6.77}$$

where the constants are $c_4 = 2.2 \times 10^3$, $c_5 = 15$, $c_6 = 1.3 \times 10^{-9}$, $c_7 = 10^{11}$, $c_8 = 10^{27}$, $c_9 = 1.3 \times 10^{-16}$, $c_{10} = 10^6$; and the exponents are $\gamma_4 = 0.306$, $\gamma_5 = -4.38$, $\gamma_6 = 2$, $\gamma_7 = 4$, $\gamma_8 = -0.36$, $\gamma_9 = 2$, and $\gamma_{10} = -0.85$. Eq. 6.77 is applied to MEM's mass range and is shown in Figure 7.

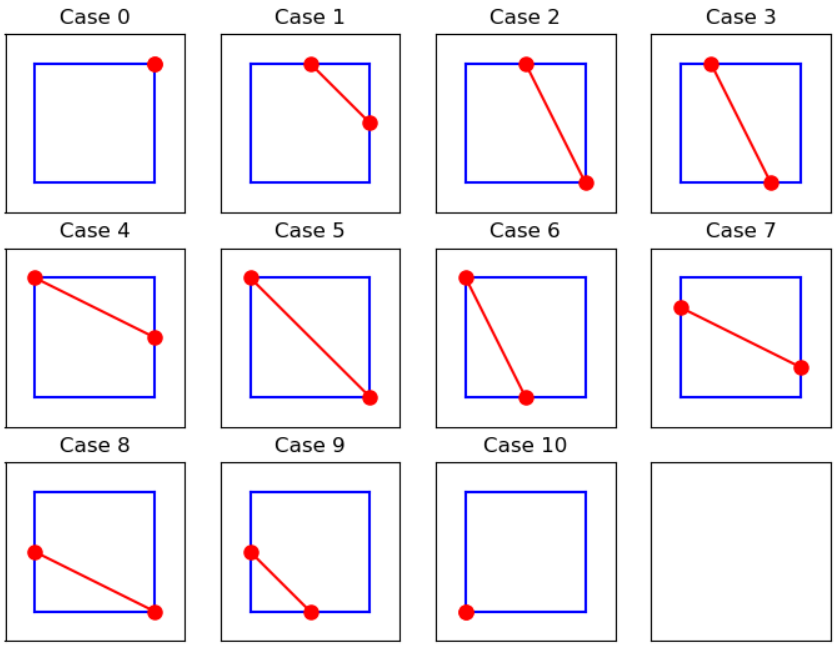


Figure 6: Illustration of the various ways a line can cross a rectangular region assuming a negative-definite slope.

The mass flux $dg(m)/dm$ and Eq. 6.10 should be integrated over the mass range $m_{min} = 10^{-6}$ g to $m_{max} = 10^{1}$ g in order to account for all impactor mass sizes, which we call $G_m$ given as

$$G_m = \int_{m_{min}}^{m_{max}} dm \frac{dg(m)}{dm} m. \tag{6.78}$$

The mass flux $dg(m)/dm$ can be fit to a double power law

$$\frac{dg(x)}{dx} = \frac{1}{ax^b + cx^d}, \tag{6.79}$$

where the fit parameters are shown in Figure 8, using a log-log scale to capture the small and large masses correctly.

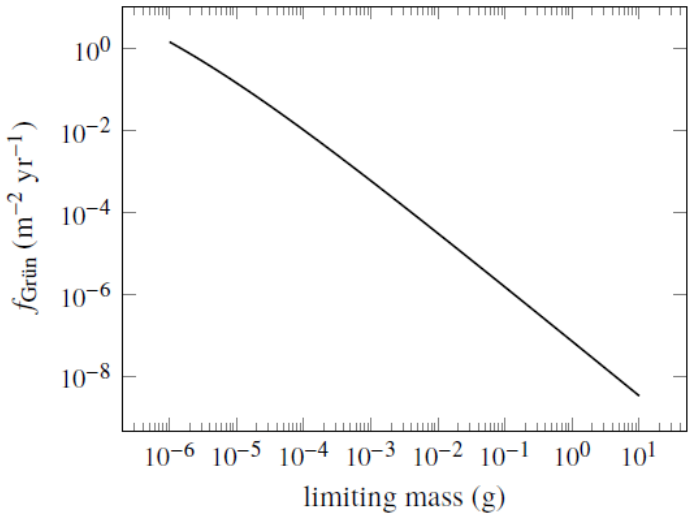


Figure 7: The Grün interplanetary meteoroid flux as a function of limiting particle mass [*Moorhead et al.*, 2019, Figure 1].

```
[1/2/2020 4:13:33 PM            Plot: "Graph4"]
Non-linear fit of dataset: Table2_2, using function: log10(1/(a*(10^x)^b+c*(10^x)^d))
Y standard errors: Unknown
Nelder-Mead Simplex algorithm with tolerance = 0.0001
From x = -5.924382925 to x = 0.935617075
a  = 321,865,117,982,837 +/- 0
b  = 2.32111297269978 +/- 0.0005958076665748
c  = 1,406,901,447,961.14 +/- 0
d  = 1.81651108891357 +/- 0.00063978048941211
Chi^2 = 0.00183119809759917
R^2 = 0.999998212686885
Iterations = 95
Status = success
```

Figure 8: Non-linear fit of Figure 7 with Eq. 6.79 in SciDAVis, giving the constants for $a$, $b$, $c$, and $d$.

To integrate Eq. (6.78), we use the following solutions

$$\int dx \frac{x}{ax^b + cx^d} = -\frac{1}{a(b-2)x^{b-2}} {}_2F_1\left[1, \frac{b-2}{b-d}; \frac{b-2}{b-d} + 1; -\frac{c}{a}x^{d-b}\right], \tag{6.80}$$

$$= -\frac{1}{c(d-2)x^{d-2}} {}_2F_1\left[1, \frac{d-2}{d-b}; \frac{d-2}{d-b} + 1; -\frac{a}{c}x^{b-d}\right], \tag{6.81}$$

where Eq. 6.80 is more appropriate for small $x$ if $d - b > 0$ and Eq. 6.81 is more appropriate for large $x$ if $d - b > 0$. If the sign of $d - b$ is flipped, then the small and large scale equations are swapped.

## 6.7 Meteoroid Projectile Density Distribution

The meteoroid density has two components, a low and a high density contribution, as shown in Figure 9. To take into account this particular distribution in computing the particle flux mass spectrum, we should integrate Figure 9 against Eq. 6.10. Since the meteoroid density components can be written in terms of log-normal distributions

$$F_\delta(x) = \frac{A}{\sigma\sqrt{2\pi}x}\exp\left[-\frac{(\ln x - \mu_\delta)^2}{2\sigma^2}\right], \tag{6.82}$$

the integration entails computing the moments of a log-normal distribution. The $\alpha$-moment is given by

$$F_\delta^\alpha(A, \mu_\delta, \sigma) = A\exp\left(\alpha\mu_\delta + \frac{1}{2}\alpha^2\sigma^2\right). \tag{6.83}$$

Inserting these results into Eq. 6.10, the functional form of the projectile density contribution can be written as

$$F_\delta = F_\delta^{3\nu-1}(A_{low}, \mu_{low}, \sigma_{low}) + F_\delta^{3\nu-1}(A_{high}, \mu_{high}, \sigma_{high}), \tag{6.84}$$

where the fit parameters for the low and high density components are shown in Figures 10 and 11. Since the meteoroid density is given in units of *fraction per 50 kg* $m^{-3}$, we need to divide the $A$ constants by 50 in order to give correct units.

## 6.8 Meteoroid Projectile Speed and Angle Distribution

MEM3 gives the incoming meteoroid flux (in units of # per km$^2$ per year) in terms of the speed $U$ and both azimuth $\theta$ and altitude $\phi$ angles for a location on the Moon. At the moment, since we are assuming azimuthally symmetric ejecta, we will sum over all $\theta$ azimuthal angles to simplify our calculation. In the future, we plan to incorporate azimuthal dependence for oblique impacts by including the azimuthal dependence of the ejecta blanket. The $\phi$ angle in MEM3 corresponds to our $\alpha$ angle, which is the impact angle with respect to the horizon. There are 36 $\phi$ bins[5] and 40 speed bins, after integrating over the 72 $\theta$ bins for each $\phi$ bin.

## 6.9 Secondary Ejecta Distance, Speed, & Angle

We would like to relate the distance from the meteorite impact to the secondary ejecta impact site by the secondary ejecta speed $v$ and angle $\gamma$ from zenith. If we assume the Moon is a perfect sphere with no atmosphere, we can calculate this distance by

[5] Half of the $\phi$ bins will always be zero, since they are below the horizon, so they can be ignored.

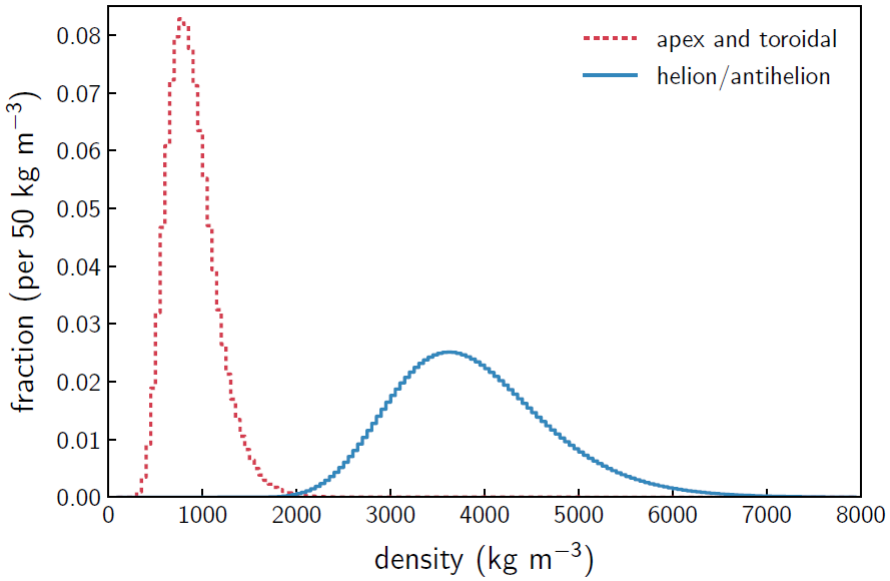


Figure 9: Meteoroid density distribution according to the MEM3 User Guide. The apex and toroidal meteoroid sources constitute the low-density population, while the helion/antihelion source constitutes the high-density population. Each set of densities follows a log-normal distribution [c.f. Figure 11, *Moorhead et al.*, 2019].

```
[1/2/2020 5:16:00 PM            Plot: "Graph5"]
Non-linear fit of dataset: Table3_2, using function: log10(a/((10^x)*s*2.506628275)*exp(-(x*ln(10)-m)^2/(2*s^2)))
Y standard errors: Unknown
Scaled Levenberg-Marquardt algorithm with tolerance = 0.0001
From x = 2.097 to x = 3.902
a  = 53.839135327051 +/- 0.82189223780795
s  = 0.294917539134767 +/- 0.000210957288819632
m  = 6.7346464600191 +/- 0.00131007263737737
Chi^2 = 0.305039664208057
R^2 = 0.999894109124399
Iterations = 0
Status = success
```

Figure 10: Non-linear fit of the low density profile in Figure 9 with Eq. 6.82 in SciDAVis, giving the constants for $a \to A$, $s \to \sigma$, and $m \to \mu_\delta$.

following the elliptical path the ejecta makes. The semi-major axis and eccentricity of

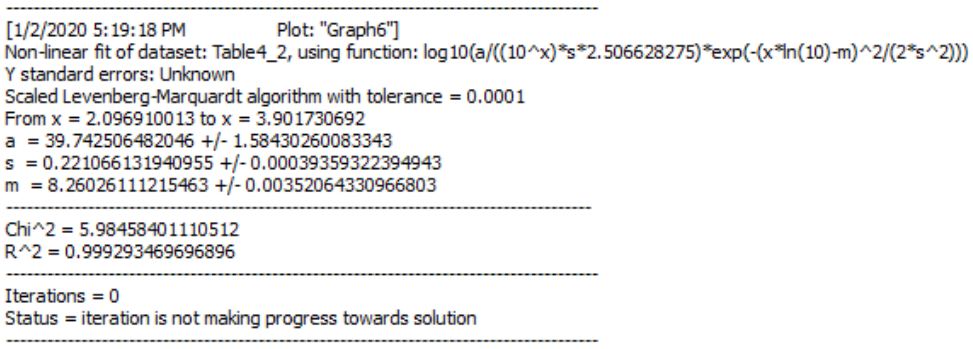


Figure 11: Non-linear fit of the high density profile in Figure 9 with Eq. 6.82 in SciDAVis, giving the constants for $a \to A$, $s \to \sigma$, and $m \to \mu_\delta$.

the elliptical orbit are given by[6]

$$\frac{a}{r_m} = \frac{1}{2\left(1 - \frac{v^2}{v_{esc}^2}\right)}, \tag{6.85}$$

where $r_m = 1737.1$ km is the radius of the Moon and $v_{esc} = 2.38$ km/s is the Moon's escape velocity, and

$$e = \sqrt{\left(\frac{2v^2}{v_{esc}^2} - 1\right)^2 \sin^2\gamma + \cos^2\gamma}, \tag{6.86}$$

where we employed the fact that the gravity of the Moon is $g = GM/r_m^2$ and the escape velocity is related by $v_{esc} = \sqrt{2gr_m}$. The third equation we need gives the location in the elliptical orbit by the angle $\beta$ from the perilune, the semi-major axis $a$, and the eccentricity $e$ by

$$r = \frac{a(1-e^2)}{1 + e\cos\beta}. \tag{6.87}$$

Solving for $\cos\beta$ in Eq. 6.87, we have

$$\cos\beta = \frac{1}{e}\left(\frac{a(1-e^2)}{r} - 1\right). \tag{6.88}$$

In addition, we also need the equation for $\sin\beta$, which is given by (using a right triangle)

$$\sin\beta = \frac{1}{e}\sqrt{e^2 - \left[\frac{a(1-e^2)}{r} - 1\right]^2}, \tag{6.89}$$

so that $\tan\beta$ is

$$\tan\beta = \frac{\sqrt{e^2 - \left[\frac{a(1-e^2)}{r} - 1\right]^2}}{\frac{a(1-e^2)}{r} - 1}. \tag{6.90}$$

[6] See Eqs. 4.30 and 4.32 from http://www.braeunig.us/space/orbmech.htm.

We found that the distance the secondary ejecta travels is given by the arc length of Moon the orbit travels greater than the radius of the Moon:

$$D = 2(\pi - \beta) r_m, \tag{6.91}$$

or solving for the angle $\beta$,

$$\beta = \pi - \frac{D}{2r_m}. \tag{6.92}$$

Using Eqs. 6.85 and 6.86, we can write

$$\frac{a}{r_m}(1 - e^2) = 2\frac{v^2}{v_{esc}^2}\sin^2\gamma, \tag{6.93}$$

so Eq. 6.90 becomes [c.f., Eq. (1) of *Vickery*, 1986]

$$\tan\left(\frac{D}{2r_m}\right) = \frac{2\frac{v^2}{v_{esc}^2}\sin\gamma\cos\gamma}{1 - 2\frac{v^2}{v_{esc}^2}\sin^2\gamma} = \frac{\frac{v^2}{v_{esc}^2}\sin(2\gamma)}{\frac{v^2}{v_{esc}^2}[\cos(2\gamma) - 1] + 1} = \frac{2\frac{v^2}{v_{esc}^2}\tan\gamma}{1 + (1 - 2\frac{v^2}{v_{esc}^2})\tan^2\gamma}. \tag{6.94}$$

For $D \ll 2r_m$, the optimum angle that gives the smallest velocity needed is $45°$. In other words, for a given velocity, the greatest distance is found by taking $\gamma = 45°$. However, if the distance $D$ is roughly the same order as the diameter of the Moon $2r_m$, ($D > 0.01 \times 2r_m$), then the optimal angle from zenith is greater than $45°$, i.e. a shallower angle to the horizon. This is because at large velocities, the curvature of the Moon comes into play. For larger velocities, there are also angles $\gamma$ that cannot reach a distance $D$. Allowable angles (in radians) that can travel a distance $D$ are defined by

$$\gamma > \frac{D}{4r_m}. \tag{6.95}$$

In other words, the maximum distance the ejecta can reach for a given angle is

$$D = 4\gamma r_m. \tag{6.96}$$

For example, from this equation we can conclude that for $\gamma < 45°$, the ejecta will not reach the antipodal point, see Figure 12.

Solving for $v$ we have

$$\frac{v}{v_{esc}} = \frac{+1}{\sqrt{\sin(2\gamma)\left(\cot\left(\frac{D}{2r_m}\right) + \tan\gamma\right)}} = \frac{+1}{\sqrt{1 + \sin(2\gamma)\cot\left(\frac{D}{2r_m}\right) - \cos(2\gamma)}}. \tag{6.97}$$

We can also solve for the zenith angle $\gamma$, given by

$$\cot\gamma = x^2\cot\left(\frac{D}{2r_m}\right) \pm \sqrt{x^4\cot^2\left(\frac{D}{2r_m}\right) + (2x^2 - 1)}, \tag{6.98}$$

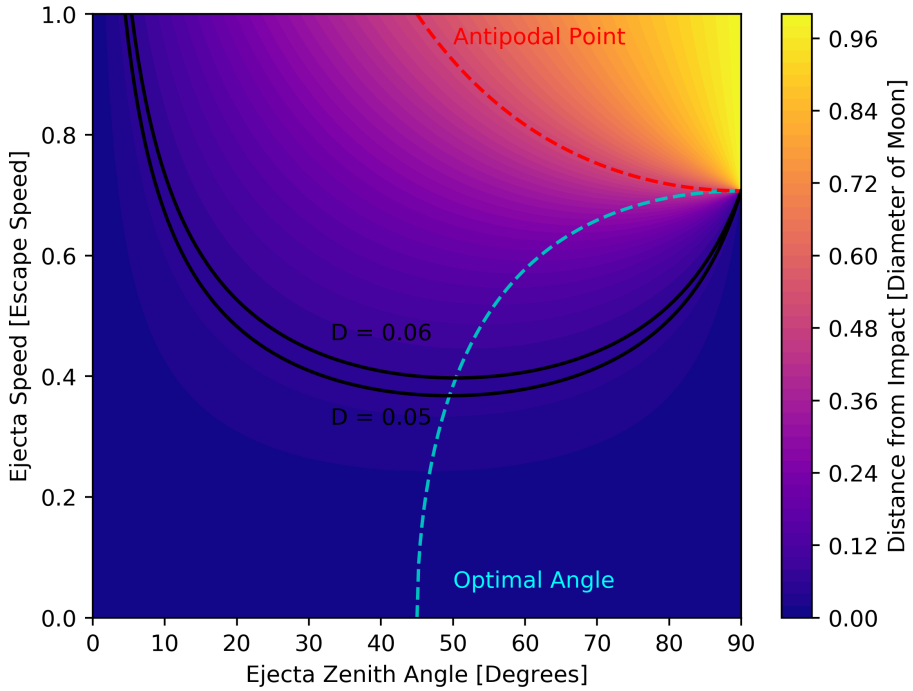


Figure 12: The color gradient shows the distance a projectile goes with a given ejected speed and zenith angle. The cyan dashed line gives the optimal angle for a given speed to reach the furthest distance, i.e., Eq. (6.101). The red dashed line shows for which pairs of speeds and zenith angles are required to hit the antipodal point. As an example, all ejecta with speed and angle pairs between the two black curves will reach a location between 0.05 and 0.06 lunar circumference units away, using Eq. (6.97).

where $x = v/v_{esc}$. Solving for the discriminant, the minimum $x$ can be for a given distance $D$ is

$$x_{min}^2 = \tan^2\left(\frac{D}{2r_m}\right)\left[\csc\left(\frac{D}{2r_m}\right) - 1\right], \tag{6.99}$$

$$= \frac{\tan\left(\frac{D}{2r_m}\right)}{\tan\left(\frac{\pi}{4} - \frac{D}{4r_m}\right)}. \tag{6.100}$$

Plugging into Equation 6.98, the optimal angle from zenith is given by

$$\begin{aligned}\cot\gamma_{opt} &= \sec\left(\frac{D}{2r_m}\right) - \tan\left(\frac{D}{2r_m}\right), \\ &= \tan\left(\frac{\pi}{4} - \frac{D}{4r_m}\right).\end{aligned} \tag{6.101}$$

Solving for $\gamma_{opt}$ we have

$$\gamma_{opt} = \frac{\pi + D/r_m}{4}, \tag{6.102}$$

which is valid for $D \leq r_m$. For larger distances, the optimal zenith angle is $\pi/2$. In terms of $x$, we have

$$\cos(2\gamma_{opt}) = \frac{x^2}{x^2-1}. \tag{6.103}$$

Once $D > \pi r_m$, the optimal angle is $\gamma = 90°$, i.e., parallel to the horizon. For small distances $D \ll 2r_m$, the optimal angle is $\gamma = 45°$, as mentioned above.

The distance traveled for the optimal angle as a function of speed is

$$\frac{D}{r_m} = \arcsin\left(\frac{x^2}{1-x^2}\right). \tag{6.104}$$

### 6.9.1 Coriolis Force

The Coriolis force on secondary ejecta may also affect the ground path. To estimate the strength of the Coriolis force, the greatest speed due to the rotation of the Moon is at the equator, given by

$$v_c = \frac{2\pi r_m}{T} = \frac{2\pi * 1737.1 \text{ km}}{27.322 \text{ days}} = 4.62 \text{ m/s}. \tag{6.105}$$

Therefore, we can ignore the Coriolis force if the ejecta speed $v$ is greater than roughly $\sim 10 - 15 \times v_c$, or about $46$ m/s to $70$ m/s. This translates into ejecta distances less than $3$ km, which at those small distances the Coriolis force should not cause an effect anyways. So in general, we conclude that we can ignore the Coriolis force all together.

To quantify this conclusion, let us compute the Rossby number

$$R_o = \frac{v}{fL}. \tag{6.106}$$

If we assume an ejecta angle of $45°$, then plotting $D$ as a function of $v$ in Eq. 6.94 shows that $D \to L \sim v^2$. Taking our example above for $v = 70$ m/s, $L = 3$ km, and $f = 2T$ to solve for $A$, we find that the Rossby number for secondary ejecta on the Moon is

$$R_o = \frac{A}{fv}, \tag{6.107}$$

where $A = 1.63$ m/s$^2$,[7] $f = 5.328 \times 10^{-6}$ rad/s, and $v$ is in units of m/s. In order to have $R_o \sim 1$ (small $R_o$ means the Coriolis forces cannot be ignored), we would need

[7] Curiously, this is basically the acceleration due to gravity on the Moon.

$v > 306$ km/s, which far exceeds the escape speed. The smallest $R_o$ can ever be is $R_o \sim 128$ when taking $v \to v_{esc}$. Therefore, we feel confident in our omission of the Coriolis force.

## 6.10 Distance and Bearing

Given two latitude-longitude points on a sphere, $(\phi_1, \theta_1)$ and $(\phi_2, \theta_2)$, we can compute the distance and bearing following Chris Veness's webpage[8].

The distance D is given by the equation

$$\tan\left(\frac{D}{2r_m}\right) = \sqrt{\frac{a}{1-a}}, \tag{6.108}$$

where $a$ is given by

$$a = \sin^2(\Delta\phi/2) + \cos\phi_1 \cos\phi_2 \sin^2(\Delta\lambda/2), \tag{6.109}$$

for $\Delta\phi = \phi_2 - \phi 1$ and $\Delta\lambda = \lambda_2 - \lambda_1$. Solving for the distance and simplifying, we have

$$D = 2r_m \arcsin(\sqrt{a}), \tag{6.110}$$

or

$$D = 2r_m \arccos(\sqrt{1-a}). \tag{6.111}$$

Other useful expressions involving trigonometric functions of $D/r_m$ are

$$\sin(D/r_m) = 2\sqrt{a(1-a)}, \tag{6.112}$$

$$\cos(D/r_m) = 1 - 2a, \tag{6.113}$$

$$\tan(D/r_m) = \frac{2\sqrt{a(1-a)}}{1-2a}. \tag{6.114}$$

Eq. (6.108) is the shortest distance between two coordinate points. For the long-distance, use

$$\tan\left(\pi - \frac{D}{2r_m}\right) = -\tan\left(\frac{D}{2r_m}\right) = \sqrt{\frac{a}{1-a}}. \tag{6.115}$$

The initial bearing $\theta$ (from due East) is given by the following equation (assuming the short-distance):

$$\tan\theta_{i(1,2)} = \frac{\sin\Delta\lambda\cos\phi_2}{\cos\phi_1\sin\phi_2 - \sin\phi_1\cos\phi_2\cos\Delta\lambda}. \tag{6.116}$$

To find the final bearing (assuming the short-distance), swap $\phi_1 \longleftrightarrow \phi_2$ and $\lambda_1 \longleftrightarrow \lambda_2$ and reverse the angle such that

$$\theta_{f(1,2)} = (\theta_{i(2,1)} + \pi) \mod 2\pi. \tag{6.117}$$

[8] https://www.movable-type.co.uk/scripts/latlong.html

In order to compute the initial and final bearing for the long-distance trajectory, add $\pi$ and then mod by $2\pi$ to Eqs. (6.116) and (6.117). In other words, swap initial and final bearings $\theta_{i(1,2)} \longleftrightarrow \theta_{f(1,2)}$.

We can also get the final latitude and longitude if we are given the distance $D$ and bearing $\theta$ from the starting location. The latitude and longitude are given by

$$\phi_2 = \arcsin\left[\sin\phi_1 \cos(D/r_m) + \cos\phi_1 \sin(D/r_m)\cos\theta\right], \tag{6.118}$$

$$\lambda_2 = \lambda_1 + \arctan\left[\frac{\sin\theta \sin(D/r_m)\cos\phi_1}{\cos(D/r_m) - \sin\phi_1 \sin\phi_2}\right]. \tag{6.119}$$

# 7 Meteoroid Ejecta Environment Output

The goal of this chapter is to outline various outputs for the lunar meteoroid ejecta environment. For each section we will provide the techniques needed to evaluate the necessary integrals. Sections 7.1 and 7.2 will be for verification purposes, Section 7.3 will be for illustration, and Section 7.4 will be the engineering environment for the revision H of DSNE, planed for the summer of 2020. The primary customer of the engineering environment will be the Appendix H contractors of the HLS (Human Landing System) Program.

## 7.1 Integral Flux ($> m$) vs. Particle Ejecta Mass

The integral flux of ejecta particles greater than mass $m$ as a function of particle ejecta mass $m$ for different ejecta speed ranges $v_i - v_{i+1}$ will aid in verifying against the NASA SP-8013 environment (Section 8) in addition to the work of Caleb Fassett (ref) and *Bjorkman and Christiansen* [2019].

## 7.2 Integral Flux ($> E_{crit}$) vs. Critical Energy

The integral flux of ejecta particles great than critical energy $E_c$ as a function of critical energy $E_c$ for different speed ranges $v_i - v_{i+1}$ will be used to compare against *Bjorkman and Christiansen* [2019].

## 7.3 Integral Flux ($> d$) vs. Particle Ejecta Size

## 7.4 Igloo Distribution of Integral Flux ($> m$)

# 8 NASA SP-8013 Meteoroid Environment Model - 1969

The NASA SP-8013 Meteoroid Environment Model [*Cour-Palais*, 1969], is a document published in 1969 that describes the meteoroid and lunar ejecta environment of cometary origin with masses between $10^{-12}$ g and $1$ g. The flux-mass models and the associated density and velocity characteristics are for engineering applications in the

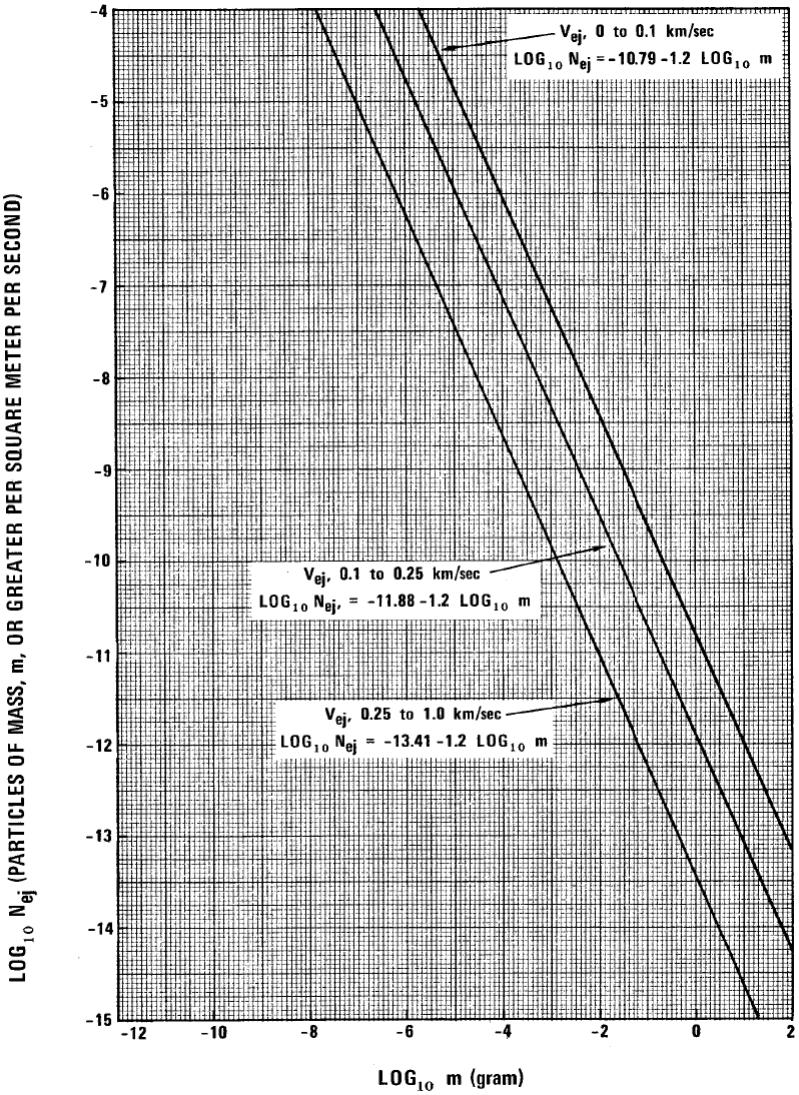


Figure 13: Average cumularive lunar ejecta flux-mass distribution for each of three ejecta velocity intervals [*Cour-Palais*, 1969].

design of space vehicles for near-Earth orbit, cis-lunar, lunar orbit, and lunar surface missions.

Our aim is to provide an updated specification to NASA SP-8013 for the lunar impact ejecta environment. Until the update is finished, DSNE points to Figure 10 (shown here in Figure 13) of *Cour-Palais* [1969] for lunar ejecta. The results that follow from Sections 5 and 6 will be verified against NASA SP-8013. We already anticipate

that our new environments will be more benign (e.g., [*Bjorkman and Christiansen*, 2019, pointing out that $50$ J is the critial energy]), however to what degree from our analysis is yet to be determined. We also plan to provide output in terms of penetrating flux as a function of critical kinetic energy, as comparison to Figure 5 of *Bjorkman and Christiansen* [2019], to aid in risk assessment of lunar impact ejecta.

Our ultimate goal in providing an updated environment definition is to have an output in the same format as MEM 3's igloo files (see Section 3.4.4 of *Moorhead et al.* [2019]). This will allow for current analysis tools already familiar with MEM 3 to ingest our new environments without modification to those tools.

### 8.1 Comparison of Scaling Laws of New and Old Ejecta Models

In this section we dive into the comparison between the scaling laws assumed in the secondary ejecta environment of the Housen & Holsapple 2011 model and the NASA SP-8013 model, i.e., *Zook* [1967]. Previously in Section 9.1, the scaling law equation from *Housen and Holsapple* [2011] has the following relation:

$$\bar{m}_{\text{HH11}}(> v) \sim \left(\frac{U}{v}\right)^{3\mu}, \tag{8.1}$$

where $\bar{m}_{\text{HH11}}(> v)$ is the secondary ejecta greater than the ejecta speed $v$, and $U$ is the impactor speed. We are ignoring any density dependence of the target or impactor. The $\mu$ index depends on the target properties (such as strength/porosity).

On the other hand, from *Zook* [1967] we have:

$$\bar{m}_{\text{Z67}}(> v) \sim U^{-2\gamma} \left[G(v)\right]^{1-\frac{3}{\alpha}(1+\gamma)}, \tag{8.2}$$

where $\gamma$ is the power-law index of the cumulative flux-mass relation of the primaries, $\alpha$ depends on the target properties, and the function $G(v)$ [from Figure 10 of *Gault et al.*, 1963] relates the dependence of ejecta mass and ejecta speed (which is assumed to be a single-valued function, such that an inverse can be defined).

## 9 Analytic Study of Secondary Lunar Ejecta

In this section, we dive into a *back-of-the-envelope* approach to understanding the secondary ejecta on the Moon. We begin by first defining the expected total mass of ejecta that is produced by an impact (or class of impacts) in Section 9.1, first discussed in Section 6.3. We then count secondary ejecta produced over the entire surface of the Moon that reaches our particular region of interest, discussed in Section 9.2.

The purpose of doing an analytic study of the secondary lunar ejecta is to compare with our computer simulations and to see mathematically what drives the secondary ejecta environment.

## 9.1 Total Ejected Mass

From *Housen and Holsapple* [2011], we can compute the mass ejected faster than $v$ in terms of impactor properties, given by (copying Equation (6.10) here for convenience))

$$M(v;\rho;m,\delta,U,\alpha) = M(>v) = C_4 m \left[\frac{v}{U\Theta(\alpha)}\left(\frac{\rho}{\delta}\right)^{\frac{3\nu-1}{3\mu}}\right]^{-3\mu}, \tag{9.1}$$

where

- $v$: secondary ejecta speed,
- $\rho$: target density,
- $m$: projectile mass,
- $\delta$: projectile density,
- $U$: projectile speed,
- $\alpha$: projectile impact angle (from horizon),

and

$$C_4 = \frac{3k}{4\pi} C_1^{3\mu}, \tag{9.2}$$

where the constants $k$, $C_1$, $\nu$, and $\mu$ depend on the specific material properties, see Table 3 of *Housen and Holsapple* [2011]. We will assume that $\Theta(\alpha) = 1$ for now (i.e., all impacts are normal to the surface), but will reintroduce this dependence later.

Given that we have a mass distribution and density distribution of primary impactors that are independent of the impact speed and other parameters, we can integrate these out. The mass term is given by (from Equation (6.78))

$$G_m = \int_{m_{min}}^{m_{max}} dm \frac{dg(m)}{dm} m. \tag{9.3}$$

where $\frac{dg(m)}{dm}$ is the derivative of the Grün interplanetary flux in Equation (6.77).

Assuming that the density distribution is log-normal, the density term is given by (from Equation (6.83))

$$F_\delta^\alpha(A,\mu_\delta,\sigma) = A\exp\left(\alpha\mu_\delta + \frac{1}{2}\alpha^2\sigma^2\right). \tag{9.4}$$

We then multiply Equation (9.1) by the primary meteor flux $f_p$ (in number per area per time) so that we have

$$M_p(>v) = \frac{C_4 G_m F_\delta^{3\nu-1}}{\rho^{3\nu-1}} f_p \left(\frac{U}{v}\right)^{3\mu}, \tag{9.5}$$

where we will use $\nu = 0.4$ and $\mu = 0.4$ for the lunar regolith. The units of $M_p(>v)$ is now mass per impact area per time.

## 9.2 Estimated Secondary Ejecta at a ROI with Normally Impacting Primaries

In order to integrate over the entire Moon, we imagine the region-of-interest (ROI) to be centered on the z-axis of a spherical coordinate system[9] with the radius of the Moon $r_m$. Therefore, this distance from the center of the ROI is defined as $D = \theta r_m$, where $\theta$ is the angle from the z-axis. The azimuthal angle is given by $\phi$, defined to rotate in the right-handed sense from the x-axis.

The differential surface area is then given by

$$dA = r_m^2 \sin\theta d\theta d\phi = r_m \sin(D/r_m) dD d\phi. \tag{9.6}$$

When integrating over the distance, we will put a placeholder function $D_{min}$ and $D_{max}$ which can be constant in the ROI distance $D$ or the secondary ejecta speed $v$ and depend on the other.

We can back out the secondary ejecta speed distribution $H(v)$ in Equation (9.5) by employing the definition given in Equation (6.59)

$$H(v) = 3\mu v^{-(3\mu+1)}, \tag{9.7}$$

such that

$$\int_v^\infty dv' H(v') = v^{-3\mu}. \tag{9.8}$$

The corresponding speeds[10] that reach a particular ROI of radius $r_{ROI}$ (or diameter $\Delta D$) at a distance $D$ can be computed by

$$\mathcal{V}(D) = \int_{v(D_0)}^{v(D_1)} dv' H(v'), \tag{9.9}$$

$$= v(D_0 = D - r_{ROI})^{-3\mu} - v(D_1 = D + r_{ROI})^{-3\mu}. \tag{9.10}$$

In the limit as $\Delta D \to 0$, or $\Delta D / r_m \ll 1$, we can approximate $\mathcal{V}$ as

$$\mathcal{V}(D) = -\Delta D f_v'(D) + \mathcal{O}(\Delta D^3), \tag{9.11}$$

with an error[11] proportional to $\Delta D^3 f_v'''$, where the function $f_v(D)$ is given by

$$f_v(D) = v_{esc}^{-3\mu} \left[1 + \sin(2\gamma)\cot\left(\frac{D}{2r_m}\right) - \cos(2\gamma)\right]^{\frac{3\mu}{2}} = v(D,\gamma)^{-3\mu}. \tag{9.12}$$

The derivative of $f_v$ with respect to $D$ can then be computed as

$$f_v'(D) = \frac{df_v(D)}{dD} = -v_{esc}^{-3\mu} \frac{3\mu}{4} \frac{\sin(2\gamma)}{\sin^2\left(\frac{D}{2r_m}\right)} \left[1 + \sin(2\gamma)\cot\left(\frac{D}{2r_m}\right) - \cos(2\gamma)\right]^{\frac{3\mu}{2}-1}. \tag{9.13}$$

[9] When we have to worry about latitudinal effects, we will need to adjust this definition.

[10] By first imposing to integrate over the speed as a function of distance, we give up the ability to study the contribution of ejecta as a function of speed. In order to do this, we must integrate first over the zenith angle space so that we have the remaining terms as a function of distance and speed.

[11] The $\Delta D^2$ terms cancel out.

The total mass per ROI area per time for a given ejecta zenith angle $\gamma$ can be computed by integrating over the sphere of the Moon

$$M_{ROI}(\gamma) = \frac{M_p(1) r_m}{\Delta D^2} \int_{D_{min}}^{D_{max}} \int_0^{2\pi} d\phi dD \sin(D/r_m) \mathcal{V}(D,\gamma) \Phi(D), \tag{9.14}$$

where $\Phi(D)$ is the fraction of azimuth field-of-view (FOV) $\Delta\beta$ from the primary impact location to the ROI location (approximated as a circle[12] of radius $\Delta D/2$). Using Napier's law for spherical triangles, the half-angle azimuth FOV can be computed by

$$\tan(\Delta\beta/2) = \frac{\tan\left(\frac{\Delta D}{2r_m}\right)}{\sin\left(\frac{D+\Delta D/2}{r_m}\right)}, \tag{9.15}$$

such that the fraction of FOV is

$$\Phi(D) = \frac{\Delta\beta}{2\pi} = \frac{1}{\pi} \arctan\left[\frac{\tan\left(\frac{\Delta D}{2r_m}\right)}{\sin\left(\frac{D+\Delta D/2}{r_m}\right)}\right]. \tag{9.16}$$

In the limit as $\Delta D \to 0$, we can approximate Equation (9.16) as[13]

$$\Phi(D) \sim \frac{\Delta D}{2\pi r_m \sin(D/r_m)}. \tag{9.17}$$

Therefore, we can see that the $\sin(D/r_m)$ and $\Delta D$ terms cancel in Equation (9.14) (which is remarkable! or was it obvious?), so that Equation (9.14) can be simplified to

$$M_{ROI}(\gamma) \sim M_p(1) \left[v(D_{min},\gamma)^{-3\mu} - v(D_{max},\gamma)^{-3\mu}\right], \tag{9.18}$$

$$\sim M_p(> v(D_{min},\gamma)) - M_p(> v(D_{max},\gamma)), \tag{9.19}$$

for $\Delta D \ll r_m$, which is in units of mass per ROI area per time. Equation (9.19) is very interesting, because it tells us that we can directly relate the total ejected mass flux at a particular primary impact location to the total secondary mass flux at the ROI, for a given secondary ejecta angle, in the limit as our ROI length scale is small compared to the radius of the Moon. If we were to introduce a zenith ejecta angle distribution, more work would be needed.

*Another remark to make, if we study the simplified integrand of Equation (9.14), we can see that the contribution of secondary ejecta as a function of distance and ejecta zenith angle is simply given by $f_v(D,\gamma) = df_v(D,\gamma)/dD$ times a $\sin\gamma$ term. When studying small angles as the limit as $\Delta D \to 0$, one must let $\gamma = \Delta D/8r_m$, which will give a finite limit.*

[12] Although, the area of the ROI is approximated as a rectangle of area $\Delta D^2$.

[13] In this case, Mathematica is our friend.

### 9.2.1 Isotropic Azimuth and $45^\circ$ Zenith Distributions

If we assume that all the ejecta is at $45^\circ$ isotropically and we are interested in ejecta of speeds greater than $v_{min}$, then the total secondary ejecta mass flux (from Equation (9.19)) at a ROI is given by

$$M_{ROI}(45^\circ) = M_p(> v_{min}) - M_p(> v_{esc}). \tag{9.20}$$

### 9.2.2 Isotropic Azimuth and Zenith Distributions

In this section, we will assume both an isotropic ejecta distribution in both azimuth and zenith angle. It is not at all obvious from the start, but it turns out that the leading term to the solution to this problem is exactly that of Equation (9.20).

Superficially, the total secondary ejecta mass flux for an isotropic zenith angle distribution is given by

$$M_{ROI,\text{isotropic}} = \frac{\int_{\gamma_{min}}^{\pi/2} d\gamma \sin\gamma M_{ROI}(\gamma)}{\int_{\gamma_{min}}^{\pi/2} d\gamma \sin\gamma}, \tag{9.21}$$

where $M_{ROI}(\gamma)$ is given in Equation (9.18). However, we need to break this integral into separate regions. In all, we need three regions defined in the speed-angle space (see Figure 12 for an example):

Region I: $\gamma_{min} = \gamma(v_{esc}, \Delta D/2)$, $\gamma_{max} = \gamma^+(v_{min}, \Delta D/2)$

Region II: $\gamma_{min} = \gamma^+(v_{min}, \Delta D/2)$, $\gamma_{max} = \gamma^-(v_{min}, \Delta D/2)$

Region III: $\gamma_{min} = \gamma^-(v_{min}, \Delta D/2)$, $\gamma_{max} = \pi/2$

**Minimum and Maximum Zenith Angles:** First, we will define the minimum and maximum zenith angles for each region.

In region I, $\gamma_{min}$ can be solved exactly and is given by (see Equation (6.96))

$$\gamma_{I,min} = \gamma(v_{esc}, \Delta D/2) = \frac{\Delta D}{8 r_m}. \tag{9.22}$$

The maximum angle $\gamma_{max}$ can be approximated by expanding Equation (6.98) for small $D \to \Delta D/2$, such that

$$\gamma_{I,max} = \gamma^+(v_{min}, \Delta D/2) \sim \frac{\Delta D}{8 r_m}\left(\frac{v_{esc}}{v_{min}}\right)^2 + \mathcal{O}\left(\frac{(\Delta D/r_m)^3}{(v_{min}/v_{esc})^6}\right), \tag{9.23}$$

for $\Delta D/r_m \ll 1$.

In region II, we minimum angle is the same as the maximum angle of the previous section, i.e.

$$\gamma_{II,min} = \gamma_{I,max}. \tag{9.24}$$

The maximum angle $\gamma_{max}$ is computed by again taking Equation (6.98) and expanding in small $D \to \Delta D/2$ so that we have

$$\gamma_{II,max} = \gamma^{-}(v_{min}, \Delta D/2) \tag{9.25}$$

$$\sim \frac{\pi}{2} - \frac{\Delta D}{8 r_m}\left(\frac{v_{esc}}{v_{min}}\right)^2 \left[1 - 2\left(\frac{v_{min}}{v_{max}}\right)^2\right] + \mathcal{O}\left(\frac{(\Delta D/r_m)^3}{(v_{min}/v_{esc})^6}\right), \tag{9.26}$$

for $\Delta D/r_m \ll 1$.

Finally, for region III, again we have the same minimum angle as the previous maximum,

$$\gamma_{III,min} = \gamma_{II,max}. \tag{9.27}$$

The maximum angle $\gamma_{max}$ is simply

$$\gamma_{II,max} = \pi/2. \tag{9.28}$$

We can already notice that in the limit as $\Delta D \to 0$, we expect the integrals in regions I and III to vanish and that the integral in region II will span zenith angles $\gamma$ from $0$ to $\pi/2$, with the limiting speeds as $v_{min}$ and $v_{max}$.

**Integration of Isotropic Zenith Angle Distribution:** We begin by breaking up the numerator of Equation (9.21) into the respective regions, so that we have

$$\begin{aligned}\int_{\gamma_{min}}^{\pi/2} d\gamma \sin\gamma M_{ROI}(\gamma) = &\int_{\gamma^{+}_{(v_{esc},\Delta D/2)}}^{\gamma^{+}_{(v_{min},\Delta D/2)}} d\gamma \sin\gamma v(\Delta D/2,\gamma)^{-3\mu} \\ &+ \int_{\gamma^{+}_{(v_{min},\Delta D/2)}}^{\gamma^{-}_{(v_{min},\Delta D/2)}} d\gamma \sin\gamma v_{min}^{-3\mu} \\ &+ \int_{\gamma^{-}_{(v_{min},\Delta D/2)}}^{\pi/2} d\gamma \sin\gamma v(\Delta D/2,\gamma)^{-3\mu} \\ &- \int_{\gamma^{+}_{(v_{esc},\Delta D/2)}}^{\pi/2} d\gamma \sin\gamma v_{esc}^{-3\mu}\end{aligned} \tag{9.29}$$

Taking the function $v(\Delta D/2,\gamma)^{-3\mu}$, as defined in Equation (6.97), and taking the limit as $\Delta D \to 0$ we have

$$v(\Delta D/2,\gamma)^{-3\mu} \sim v_{esc}^{-3\mu}\left(\frac{\sin(2\gamma)}{\sin\left(\frac{\Delta D}{4r_m}\right)}\right)^{3\mu/2}\left[1 + \mathcal{O}\left(\sin\left(\frac{\Delta D}{4r_m}\right)\frac{1-\cos(2\gamma)}{\sin(2\gamma)}\right)\right], \tag{9.30}$$

as $\Delta D \to 0$. We decided to actually expand in terms of $\sin(x)$ instead of $x$, for $x = \Delta D/4r_m$. Now we need to further expand Equation (9.30) as $\gamma \to 0$ and $\gamma \to \pi/2$.

For the first limit, we have

$$\sin\gamma v(\Delta D/2,\gamma)^{-3\mu} \sim v_{esc}^{-3\mu}\gamma\left(\frac{8\gamma r_m}{\Delta D}\right)^{3\mu/2}\left[1 + \mathcal{O}(\gamma^2, \gamma\Delta D, \Delta D^2)\right], \tag{9.31}$$

as $\Delta D \to 0$ and $\gamma \to 0$.

For the second limit, we have

$$\sin\gamma v(\Delta D/2,\gamma)^{-3\mu} \sim v_{esc}^{-3\mu}\left(\frac{8\gamma' r_m}{\Delta D}\right)^{3\mu/2}\left[\left(1+\frac{\Delta D}{4\gamma' r_m}\right)^{3\mu/2}+\mathcal{O}(\gamma^2,\gamma\Delta D,\Delta D^2)\right], \tag{9.32}$$

as $\Delta D \to 0$ and $\gamma' \to 0$, where $\gamma = \pi/2 - \gamma'$.

The first integral in region I can then be shown to be

$$\int_{\gamma^+_{(v_{esc},\Delta D/2)}}^{\gamma^+_{(v_{min},\Delta D/2)}} d\gamma \sin\gamma v(\Delta D/2,\gamma)^{-3\mu} \sim v_{esc}^{-3\mu}\int_{\frac{\Delta D}{8r_m}}^{\frac{\Delta D}{8r_m}\left(\frac{v_{esc}}{v_{min}}\right)^2} d\gamma\gamma\left(\frac{8\gamma r_m}{\Delta D}\right)^{3\mu/2}, \tag{9.33}$$

$$\sim v_{esc}^{-3\mu}\frac{\left(\frac{v_{esc}}{v_{min}}\right)^{3\mu+4}-1}{32(3\mu+4)}\frac{\Delta D}{r_m}, \tag{9.34}$$

as $\Delta D \to 0$.

In region II, our integral is much easier to evaluate, and is given by

$$\int_{\gamma^+_{(v_{min},\Delta D/2)}}^{\gamma^-_{(v_{min},\Delta D/2)}} d\gamma \sin\gamma v_{min}^{-3\mu} \sim v_{min}^{-3\mu}\int_{\frac{\Delta D}{8r_m}\left(\frac{v_{esc}}{v_{min}}\right)^2}^{\pi/2-\frac{\Delta D}{8r_m}\left(\frac{v_{esc}}{v_{min}}\right)^2\left[1-2\left(\frac{v_{min}}{v_{esc}}\right)^2\right]} d\gamma\sin\gamma, \tag{9.35}$$

$$\sim v_{min}^{-3\mu}\left[1+\frac{1}{8}\left(2-\frac{v_{esc}^2}{v_{min}^2}\right)\frac{\Delta D}{r_m}+\mathcal{O}(\Delta D^2 v_{esc}^4/v_{min}^4)\right], \tag{9.36}$$

as $\Delta D \to 0$.

The next integral in region III, is similar to that of region I. We find that the integral is given by

$$\int_{\gamma^-_{(v_{min},\Delta D/2)}}^{\pi/2} d\gamma \sin\gamma v(\Delta D/2,\gamma)^{-3\mu}, \tag{9.37}$$

$$\sim v_{esc}^{-3\mu}\int_{\pi/2-\frac{\Delta D}{8r_m}\left(\frac{v_{esc}}{v_{min}}\right)^2\left[1-2\left(\frac{v_{min}}{v_{esc}}\right)^2\right]}^{\pi/2} d\gamma\left(2+\frac{8(\pi/2-\gamma)}{\Delta D/r_m}\right)^{3\mu/2}, \tag{9.38}$$

$$\sim v_{esc}^{-3\mu}\frac{\left(\frac{v_{esc}}{v_{min}}\right)^{3\mu+2}-2^{3\mu/2+1}}{4(3\mu+2)}\frac{\Delta D}{r_m}, \tag{9.39}$$

as $\Delta D \to 0$.

Finally, the last integral that spans all regions is like the integral in region II and only requires a simple integral over $\sin$. Therefore, we have

$$\int_{\gamma^+_{(v_{esc},\Delta D/2)}}^{\pi/2} d\gamma \sin\gamma v_{esc}^{-3\mu} \sim v_{esc}^{-3\mu}\int_{\frac{\Delta D}{8r_m}}^{\pi/2} d\gamma\sin\gamma, \tag{9.40}$$

$$\sim v_{esc}^{-3\mu}\left(1-\frac{\Delta D^2}{128 r_m^2}+\mathcal{O}(\Delta D^4)\right), \tag{9.41}$$

as $\Delta D \to 0$.

Putting everything together, to first order in $\Delta D$, we finally have

$$M_{ROI,\text{isotropic}} \sim v_{min}^{-3\mu}\left[1+\frac{1}{8}\left(2-\frac{v_{esc}^2}{v_{min}^2}\right)\frac{\Delta D}{r_m}\right] - v_{esc}^{-3\mu}\left[1-\left[\frac{\left(\frac{v_{esc}}{v_{min}}\right)^{3\mu+4}-1}{32(3\mu+4)}+\frac{\left(\frac{v_{esc}}{v_{min}}\right)^{3\mu+2}-2^{3\mu/2+1}}{4(3\mu+2)}\right]\frac{\Delta D}{r_m}\right] + \mathcal{O}(\Delta D^2), \tag{9.42}$$

as $\Delta D \to 0$. If the ROI length scale $\Delta D$ is to be finite, then we require

$$\frac{\Delta D}{r_m}\left(\frac{v_{esc}}{v_{min}}\right)^4 \ll 1, \tag{9.43}$$

in order for Equation (9.42) to stay valid. The driving contribution to the integral is all from region II, since regions I and III disappear as $\Delta D \to 0$. Note that we account for ejecta that travels less than and greater than half the lunar circumference $\pi r_m$.

We can now relate the total secondary ejecta mass flux for an isotropic zenith angle distribution to be the same as if the zenith angle distribution has a delta function at $45^\circ$,

$$M_{ROI,\text{isotropic}} \sim M_{ROI}(45^\circ) + \mathcal{O}\left[\frac{\Delta D}{r_m}\left(\frac{v_{esc}}{v_{min}}\right)^4\right]. \tag{9.44}$$

## 9.3 Secondary Ejecta at a ROI vs. Distance

We are also interested in studying the contribution of secondary ejecta as a function of distance from the ROI. Instead of integrating over the distances and then integrate over the ejecta angles, we will first integrate over the ejecta zenith angles such that

$$M_{ROI}(D) = -M_p(1)\int_{D/4r_m}^{\pi/2} d\gamma \sin\gamma f_v'(D,\gamma), \tag{9.45}$$

where $f_v'(D,\gamma)$ is given in Equation (9.13). We notice that for all $\gamma$ in our domain, the integrand is strongly peaked for $D \ll r_m$ and is also dominated by $\gamma$ near $\pi/4$ or $45^\circ$.

For small $D$, we can write (using $a = 3\mu/2$)

$$\left[1+\sin(2\gamma)\cot\left(\frac{D}{2r_m}\right)-\cos(2\gamma)\right]^{a-1} \sim \left[\frac{\sin(2\gamma)}{D/2r_m}\right]^{a-1}, \tag{9.46}$$

as $D \to 0$. Therefore, we can write Equation (9.45) as

$$M_{ROI}(D) \sim aM_p(>v_{esc})\int_{D/4r_m}^{\pi/2} d\gamma \frac{\sin\gamma\sin(2\gamma)}{\sin^2\left(\frac{D}{2r_m}\right)}\left[\frac{\sin(2\gamma)}{D/2r_m}\right]^{a-1}, \tag{9.47}$$

as $D \rightarrow 0$. Collecting the $\gamma$-dependent terms, we let $x = \cos\gamma$ such that $dx = -\sin\gamma d\gamma$,

$$\int_{D/4r_m}^{\pi/2} d\gamma \sin\gamma \sin^a(2\gamma) = 2^a \int_0^{\cos(D/4r_m)} dx x^a (1-x^2)^{a/2}. \tag{9.48}$$

We employ another substitution $y = x^2$ such that $dx = dy/2\sqrt{y}$, giving

$$= 2^{a-1} \int_0^{\cos^2(D/4r_m)} dy y^{\frac{a-1}{2}} (1-y)^{a/2} = 2^{a-1}\beta\left(\cos^2(D/4r_m), \frac{a+1}{2}, \frac{a}{2}+1\right), \tag{9.49}$$

and we notice that this is the integral for the incomplete beta function. Therefore, the contribution of secondary ejecta as a function of distance is given by (replacing $D/4r_m$ by $\tan(D/4r_m)$)

$$M_{ROI}(D) \sim M_p(>v_{esc}) \frac{3\mu}{2} \frac{\cot\left(\frac{D}{4r_m}\right)^{3\mu/2-1}}{\sin^2\left(\frac{D}{2r_m}\right)} \beta\left(\cos^2(D/4r_m), \frac{3\mu+2}{4}, \frac{3\mu}{4}+1\right), \tag{9.50}$$

$$\sim M_p(>v_{esc}) \frac{3\mu}{8} \frac{\Gamma\left(\frac{3\mu+2}{4}\right)\Gamma\left(\frac{3\mu}{4}+1\right)}{\Gamma\left(\frac{3\mu+3}{2}\right)} \left(\frac{D}{4r_m}\right)^{-(3\mu/2+1)}, \tag{9.51}$$

We do note that the normalization factor should not be taken seriously in this calculation. If one then integrates over the entire Moon using Equation (9.51), an overestimate of about a factor of $2.29$ will occur. The point is to illustrate that the contribution roughly follows a power law of index $-(3\mu/2+1)$, which for $\mu = 0.4$, the index is $-1.6$. To compare with the speed distribution $H(v)$, the power law index would be $-(3\mu+1) = -2.2$.

## 9.4 Secondary Ejecta at a ROI vs. Speed for a given Distance

To study the speed distribution as a function of distance, we begin with the speed distribution $H(v)$ and integrate over all contributing angles. For this exercise, we will assume an isotropic distribution. For a given distance and speed, the zenith angle dependence is a multi-valued function for speeds $v/v_{esc} < \sqrt{2}/2$ and a single-valued function for speeds $v/v_{esc} \geq \sqrt{2}/2$.

The integral over the secondary ejecta as a function of speed and distance is given by

$$M_{ROI}(D,v) = dA(D)\Phi(D)H(v) \int_{\gamma_{min}}^{\gamma_{max}} d\gamma \sin\gamma. \tag{9.52}$$

We must break up the integral over the zenith angle into two regions in order to have a single-valued function, one less than the optimal angle $\gamma_{opt}$ and one greater than. In the limit as the ROI size goes to zero, the region between the two cases goes away, so we will not worry about it here. Breaking up the integral, we have (assuming[14]

[14]The $v_{min}$ defined here is different from previous usage in Section 9.

$v > v_{min}$)

$$\int_{\gamma_{min}}^{\gamma_{max}} d\gamma \sin\gamma = \int_{\gamma^+(D_1,v)}^{\gamma^+(D_0,v)} d\gamma \sin\gamma + \begin{cases} \int_{\gamma^-(D_1,v)}^{\gamma^-(D_0,v)} d\gamma \sin\gamma & \text{for } D \leq \pi r_m \text{ and } \frac{v^2}{v_{esc}^2} \leq \frac{1}{2} \\ 0 & \text{for } D > \pi r_m \text{ or } \frac{v^2}{v_{esc}^2} > \frac{1}{2} \end{cases}, \tag{9.53}$$

where $D_0 = D - \Delta D/2$ and $D_1 = D + \Delta D/2$ with the ROI width diameter of $\Delta D$. We also note that the minimum speed $v_{min}$ for a given distance $D$ is given by (see also Equation (6.100))

$$\frac{v_{min}^2}{v_{esc}^2} = \frac{\tan\left(\frac{D}{2r_m}\right)}{\tan\left(\frac{\pi}{4} - \frac{D}{4r_m}\right)}. \tag{9.54}$$

The angles $\gamma^\pm$ are given by (see Equation (6.98))

$$\cot\gamma^\pm = x^2 \cot\left(\frac{D}{2r_m}\right) \pm \sqrt{x^4 \cot^2\left(\frac{D}{2r_m}\right) + (2x^2 - 1)}. \tag{9.55}$$

Evaluating the integrals and letting $\Delta D \to 0$, we arrive at the following solution:

$$M_{ROI}(D, v) \sim dA(D)\Phi(D)H(v)\Delta D\mathcal{G}(D, v), \tag{9.56}$$

where the geometrical term of the secondary ejecta speed distribution is (see Figure 14 for an example)

$$\mathcal{G}(D, v) \sim \begin{cases} -\frac{d}{dD}\cos\gamma^+ + \frac{d}{dD}\cos\gamma^- & \text{for } D \leq \pi r_m \text{ and } \frac{v_{min}^2}{v_{esc}^2} \leq \frac{v^2}{v_{esc}^2} \leq \frac{1}{2} \\ -\frac{d}{dD}\cos\gamma^+ & \text{for } D > \pi r_m \text{ or } \frac{v^2}{v_{esc}^2} > \frac{1}{2} \\ 0 & \text{for } \frac{v^2}{v_{esc}^2} < \frac{v_{min}^2}{v_{esc}^2}, \end{cases} \tag{9.57}$$

for $\Delta D \to 0$ and the $\cos\gamma^\pm$ terms can be computed from the $\cot\gamma^\pm$ equation by

$$\cos\gamma^\pm = \frac{\cot\gamma^\pm}{\sqrt{1 + \cot^2\gamma^\pm}}. \tag{9.58}$$

In Figure 14, we can see that for distances less than $\pi r_m$, i.e. less than half the lunar circumference, the speed distribution decreases for larger speeds. However, for distances greater than half the lunar circumference, only speeds $v > \frac{\sqrt{2}}{2} v_{esc}$ are valid and the speed distribution increases for larger speeds. The fastest speeds near the escape speed seem to be more prevalent from distances $D > \pi r_m$. It is also evident that the ejecta originating from close distances dominates the total secondary ejecta.

Not shown in Figure 14 due to plotting artifacts and scaling, the peaks as a function of speed are proportional to $\propto v^{-2}$ for speeds $v < \frac{\sqrt{2}}{2} v_{esc}$

## 9.5 Secondary Ejecta at a Satellite of the Moon

In this section, we will derive more general equations than what was done in Section 6.9 by assuming the final impact radius to be different from the ejected radius,

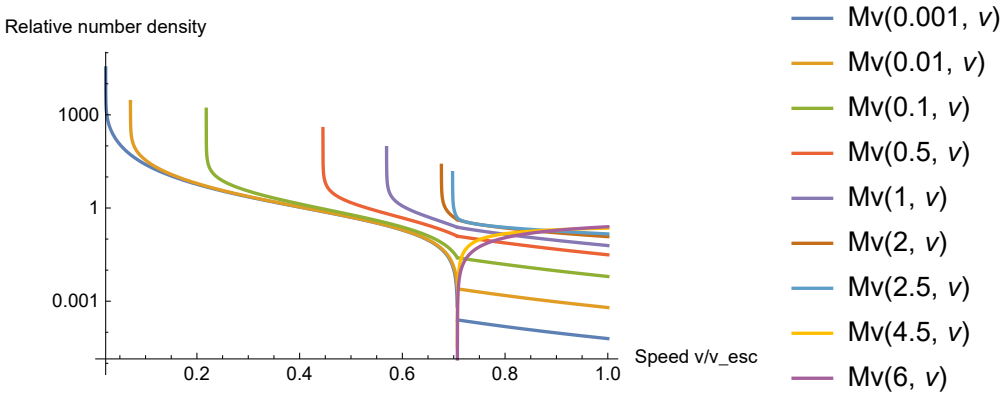


Figure 14: The geometrical term of the secondary ejecta speed distribution $\mathcal{G}(D, v)$ as a function of speed for various distances in units of lunar radii $r_m$.

where before we assumed the heights were the same. For convenience, we rewrite Equations (6.85), (6.86), and (6.87) here:

$$\frac{a}{r_m} = \frac{1}{2\left(1 - \frac{v^2}{v_{esc}^2}\right)}, \tag{9.59}$$

where $r_m = 1737.1$ km is the radius of the Moon and $v_{esc} = 2.38$ km/s is the Moon's escape velocity, and

$$e = \sqrt{\left(\frac{2v^2}{v_{esc}^2} - 1\right)^2 \sin^2\gamma + \cos^2\gamma}, \tag{9.60}$$

where we employed the fact that the gravity of the Moon is $g = GM/r_m^2$ and the escape velocity is related by $v_{esc} = \sqrt{2gr_m}$. The third equation we need gives the location in the elliptical orbit by the angle $\beta$ from the perilune, the semi-major axis $a$, and the eccentricity $e$ by

$$r = \frac{a(1 - e^2)}{1 + e\cos\beta}. \tag{9.61}$$

We will define the $p$-subscripts by the particle ejecta location and the $s$-subscripts by the satellite location. Unless stated otherwise, we will assume the ejecta speed $v_p$ and zenith angle $\gamma_p$ are given in addition to the satellite radius $r_s$ from the center of the Moon.

**Satellite Angle from Periapsis** The satellite location with respect to the perilune $\beta_s$ has a similar structure to that of the location of the ejecta $\beta_p$, given by

$$\tan\beta_s = \frac{2\frac{v_p^2}{v_{esc}^2}\sin\gamma_p\cos\gamma_p}{2\frac{r_m}{r_s}\frac{v_p^2}{v_{esc}^2}\sin^2\gamma_p - 1} F_s(r_s, v_p, \gamma_p), \tag{9.62}$$

where the factor $F_s$ is given by

$$F_s(r_s, v_p, \gamma_p) = \sqrt{1 + \frac{1 - \frac{r_m}{r_s}}{\cos^2 \gamma_p} \left[ \sin^2 \gamma_p \left( 1 + \frac{r_m}{r_s} \right) - \frac{v_{esc}^2}{v_p^2} \right]}. \tag{9.63}$$

**Ejecta Local Zenith Angle at Satellite** The local zenith angle of the ejecta at the satellite $\gamma_s$ starts from

$$\tan\left(\frac{\pi}{2} - \gamma_s\right) = \frac{e \sin \beta_s}{1 + e \cos \beta_s}, \tag{9.64}$$

where

$$e \cos \beta_s = \frac{a}{r_s}(1 - e^2) - 1 \tag{9.65}$$

$$= 2\frac{r_m}{r_s}\frac{v_p^2}{v_{esc}^2} \sin^2 \gamma_p - 1, \tag{9.66}$$

$$e \sin \beta_s = \sqrt{e^2 - (e \cos \beta_s)^2} \tag{9.67}$$

$$= 2\frac{v_p^2}{v_{esc}^2} \sin \gamma_p \cos \gamma_p F_s(r_s, v_p, \gamma_p), \tag{9.68}$$

such that

$$\cot \gamma_s = \frac{r_s}{r_m} \cot \gamma_p F_s(r_s, v_p, \gamma_p). \tag{9.69}$$

**Maximum Apoapsis of Ejecta** The maximum height $r_{\text{max}}$ (i.e., the apoapsis) the ejecta of speed $v_p$ and zenith angle $\gamma_p$ is given by (fixing the typo in Equation 16 of *Gault et al.* [1963])

$$\frac{r_{\text{max}}}{r_m} = \frac{1 + \sqrt{1 - 4\frac{v_p^2}{v_{esc}^2}\left(1 - \frac{v_p^2}{v_{esc}^2}\right)\sin^2 \gamma_p}}{2\left(1 - \frac{v_p^2}{v_{esc}^2}\right)} \tag{9.70}$$

**Restriction of Ejecta Speed for known Satellite Height and Ejecta Angle** To reach a particular satellite radius $r_s = r_{\text{max}}$ for a given ejecta angle $\gamma_p$, we have the following condition on the ejecta speed $v_p$:

$$\frac{v_p}{v_{esc}} = \sqrt{\frac{\frac{r_{\text{max}}}{r_m}\left(\frac{r_{\text{max}}}{r_m} - 1\right)}{\frac{r_{\text{max}}^2}{r_m^2} - \sin^2 \gamma_p}}. \tag{9.71}$$

To find the speed of the ejecta at the satellite height, use the following expression.

**Ejecta Speed at Satellite** The speed of the ejecta at the satellite orbital radius given the initial ejecta speed is given by

$$\frac{v_s}{v_{esc}} = \sqrt{\frac{r_m}{r_s} + \frac{v_p^2}{v_{esc}^2} - 1}. \tag{9.72}$$

If $r_s \to \infty$, then $v_\infty$ is the hyperbolic excess speed

$$\frac{v_\infty}{v_{esc}} = \sqrt{\frac{v_p^2}{v_{esc}^2} - 1}. \tag{9.73}$$

Rearranging to solve for the ejecta speed $v_p$, we have

$$\frac{v_p}{v_{esc}} = \sqrt{1 - \frac{r_m}{r_s} + \frac{v_s^2}{v_{esc}^2}}. \tag{9.74}$$

**Geographic Distance between Impact Point and Satellite** The geographic distance between the point of primary impact and the satellite $D_s$ can be related between the difference between angles from periapsis

$$\frac{D_s}{r_m} = \beta_s - \beta_p. \tag{9.75}$$

Taking the tangent of this difference, we can use Equations (9.62) and (6.94) for the satellite and point-of-impact (POI) periapsis angles $\beta_s$ and $\beta_p$ such that

$$\begin{aligned} \tan\left(\frac{D_s}{r_m}\right) &= \tan(\beta_s - \beta_p) \\ &= \frac{\tan\beta_s - \tan\beta_p}{1 + \tan\beta_s \tan\beta_p} \end{aligned} \tag{9.76}$$

In terms of the satellite angle from periapsis $\beta_s$, we have

$$\tan\beta_s = \frac{\tan(D_s/r_m) + \tan\beta_p}{1 - \tan(D_s/r_m)\tan\beta_p}. \tag{9.77}$$

We could then assume a specific location of the satellite defined by it's height and geographic distance from the POI and find the valid ejecta angles and speeds.

# References

Bjorkman, M. D., and E. L. Christiansen, An astronaut's risk of experiencing a critical impact from lunar ejecta during lunar eva, *First Int'l. Orbital Debris Conf.*, 2019.

Bouley, S., et al., Power and duration of impact flashes on the moon: Implication for the cause of radiation, *Icarus*, *218*(1), 115–124, 2012.

Brown, P., R. Spalding, D. O. ReVelle, E. Tagliaferri, and S. Worden, The flux of small near-earth objects colliding with the earth, *Nature*, *420*(6913), 294, 2002.

Carrier, W. D., Lunar soil grain size distribution, *The moon*, *6*(3-4), 250–263, 1973.

Carrier III, W. D., Particle size distribution of lunar soil, *Journal of Geotechnical and Geoenvironmental Engineering*, *129*(10), 956–959, 2003.

Cour-Palais, B. G., Meteoroid environment model 1969 (near earth to lunar surface), nasa sp-8013, *National Aeronautics and Space Administration, Washington, DC*, 1969.

Gault, D. E., Impact cratering, in *A primer in lunar geology*, 1974.

Gault, D. E., and J. A. Wedekind, Experimental studies of oblique impact, in *Lunar and Planetary Science Conference Proceedings*, vol. 9, pp. 3843–3875, 1978.

Gault, D. E., E. M. Shoemaker, and H. J. Moore, *NASA TN D-1767 Spray ejected from the lunar surface by meteoroid impact*, National Aeronautics and Space Administration, 1963.

Grün, E., H. Zook, H. Fechtig, and R. Giese, Collisional balance of the meteoritic complex, *Icarus*, *62*(2), 244–272, 1985.

Holsapple, K., The scaling of impact processes in planetary sciences, *Annual review of earth and planetary sciences*, *21*(1), 333–373, 1993.

Housen, K. R., and K. A. Holsapple, Ejecta from impact craters, *Icarus*, *211*(1), 856–875, 2011.

Miller, A., Esabase2 debris release 10.0 technical description, *Tech. Rep. 1.7*, ESA, 2017.

Moorhead, A. V., A. Kingery, and S. Ehlert, Nasa's meteoroid engineering model 3 and its ability to replicate spacecraft impact rates, *Journal of Spacecraft and Rockets*, pp. 1–17, 2019.

Moser, D., R. Suggs, W. Swift, R. Suggs, W. Cooke, A. Diekmann, and H. Koehler, Luminous efficiency of hypervelocity meteoroid impacts on the moon derived from the 2006 geminids, 2007 lyrids, and 2008 taurids, *Meteoroids: The Smallest Solar System Bodies*, p. 142, 2011.

Moser, D., R. Suggs, and R. Suggs, Large meteoroid impact on the moon on 17 march 2013, in *Asteroids, Comets, Meteors 2014*, 2014.

Neukum, G., B. A. Ivanov, and W. K. Hartmann, Cratering records in the inner solar system in relation to the lunar reference system, in *Chronology and evolution of Mars*, pp. 55–86, Springer, 2001.

Rival, M., and J. Mandeville, Modeling of ejecta produced upon hypervelocity impacts, *Space debris*, *1*(1), 45–57, 1999.

Robinson, M. S., et al., New crater on the moon and a swarm of secondaries, *Icarus*, *252*, 229–235, 2015.

Shuvalov, V., Ejecta deposition after oblique impacts: An influence of impact scale, *Meteoritics & Planetary Science*, *46*(11), 1713–1718, 2011.

Vickery, A., Size-velocity distribution of large ejecta fragments, *Icarus*, *67*(2), 224–236, 1986.

Zook, H. A., The problem of secondary ejecta near the lunar surface., in *Transactions of the 1967 National Symposium on Saturn V/Apollo and Beyond*, vol. I, pp. EN–8, 1967.